Robertson, A.H.F., Emeis, K.-C., Richter, C., and Camerlenghi, A. (Eds.), 1998
Proceedings of the Ocean Drilling Program, Scientific Results, Vol. 160

4. CONTINUOUS SEDIMENTARY SEQUENCES FROM THE EASTERN MEDITERRANEAN SEA: COMPOSITE DEPTH SECTIONS[1]

Tatsuhiko Sakamoto,[2] Thomas Janecek,[3] and Kay-Christian Emeis[4]

ABSTRACT

We have developed revised postcruise composite depth sections over the ~100-m-long, Pliocene–Holocene sediment sequences at four paleoceanographic sites (Site 964: Ionian Basin; Sites 966 and 967: Eratosthenes Seamount; Site 969: Mediterranean Ridge), which are located in different tectonic and oceanographic settings and water depths in the Eastern Mediterranean Sea. These revised composite sections were constructed using correlation intervals of a few centimeters instead of the 1- to 10-m intervals used in the shipboard composite construction procedure. These revised composite depth sections now take into account differential stretching and squeezing within a core and correct depth differences between holes caused by coring artifact and tectonic disturbances that resulted in attenuated and incomplete sections. The revised composite depth sections were constructed by combining digitized color images of split cores, visual core descriptions from shipboard operations, and color reflectance measurements with a 2-cm sampling resolution. The detailed revised depth sequences not only enable us to correlate sapropels between holes, but also other lithofacies, such as pale nannofossil oozes, reddish oozes, dark clays, and ash layers. Depending on the location of the drill site, over 80 individual sapropels are recognized in the revised composite depth sections. During Leg 160, use of the advanced piston coring system on the *JOIDES Resolution* typically resulted in an average gap between cores of 1–2 m, with a maximum of 8 m. Gaps within cores, resulting from faulting, slumping, or mass flows, also averaged 1–2 m in length. These revised composite depth sections can be used as starting points for the development of high-resolution time scales and paleoceanographic time series in the Mediterranean.

INTRODUCTION

The paleoceanographic objectives of Leg 160 were (1) to investigate external and internal forcing mechanisms of sapropel formation in relation to global and regional variations in atmospheric circulation and water-mass variability since the Pliocene; (2) to establish variations in environmental conditions at each site, as recorded in geochemical, paleontological, and isotopic proxy indicators for water-column stratification, paleo-oxidation-reduction conditions, and paleoproductivity levels; and (3) to examine the spatial gradients in environmental conditions for coeval sapropels along an east–west transect of drill sites. The east–west transect permits reconstruction of gradients and patterns in depositional, paleoceanographic, and climatic conditions for the entire basin in high resolution. The gradients and patterns allow us to determine the driving forces behind sapropel formation at different times, and to determine how the physical circulation and chemical cycling preconditioned the Mediterranean Sea toward sapropel formation.

Leg 160 drill sites were selected to core along the eastern limb of an east–west transect across the entire eastern Mediterranean Sea (Fig. 1) to achieve these objectives and to fulfill three essential requirements. The first requirement was stratigraphic continuity. Sedimentary sections at paleoceanographic sites must be complete, undisturbed, and shielded from the occasionally drastic effects of submarine morphology and tectonics of the Mediterranean Sea. The second requirement was optimum areal and water-mass coverage. The drill sites must cover the entire Mediterranean basin to permit evaluation of paleoceanographic, paleochemical, and paleontological zonality throughout the entire basin. The third requirement was the recovery of enough material from multiple holes to permit centimeter- to millimeter-scale sampling densities in the sapropel layers, as well as in the normal sediments immediately above and below the sapropels.

One of the most important improvements of Leg 160, in comparison with previous drilling legs in the Mediterranean Sea (Deep Sea Drilling Project [DSDP] Legs 13, 42A, and Ocean Drilling Program [ODP] Leg 107) lies with the recovery of continuous hemipelagic sequences that include more than 80 discrete sapropels. The prime reason for success was the high core recovery achieved by multiple advanced piston coring (APC). However, we found that interhole and intersite correlation was hardly trivial: diagenetic and tectonic processes had significant effects on the recovered cores, and drilling artifacts were abundant (Emeis, Robertson, Richter, et al., 1996). The effects of these disruptive processes necessitated construction of postcruise, high-resolution composite depth sections to verify continuity in each sequence drilled and to provide the best available starting point for high-resolution stratigraphies, including micropaleontological, paleomagnetic, tephrachronological, and isotopic studies (Howell et al., Chap. 13, this volume; Kroon et al., Chap. 14, this volume; Staerker, Chap. 7, this volume; di Stefano et al., Chap. 8, this volume).

Since the initial use of hydraulic piston coring (HPC) during DSDP Leg 68 and APC coring during DSDP Leg 94, excellent core recovery has made high-resolution Cenozoic paleoceanography possible. Although most APC core recovery averaged over 100% during Leg 160, gaps on the order of 1 to 2 m were common. These coring problems and possible causes were reported and discussed from many previous DSDP and ODP legs, including Leg 69 (Shackleton and Hall, 1983), Leg 94 (Ruddiman et al., 1987; Ruddiman et al., 1989; Raymo et al., 1989), Leg 111 (Alexandrovitch and Hays, 1989), Leg 115 (Robinson, 1990), Leg 117 (deMenocal et al., 1991; Murray and Prell, 1991), Leg 121 (Farrell and Janecek, 1991), Leg

[1]Robertson, A.H.F., Emeis, K.-C., Richter, C., and Camerlenghi, A. (Eds.), 1998. *Proc. ODP, Sci. Results*, 160: College Station, TX (Ocean Drilling Program).

[2]Department of Earth and Planetary Sciences, Hokkaido University, Sapporo, Japan. tats@cosmos.sci.hokudai.ac.jp

[3]Antarctic Marine Geology Research Facility, Florida State University, Tallahassee, Florida, U.S.A.

[4]Institut für Ostseeforschung Warnemünde, Seestrasse 15, D-18119 Warnemünde, Federal Republic of Germany.

Prior Chapter Contents Next Chapter

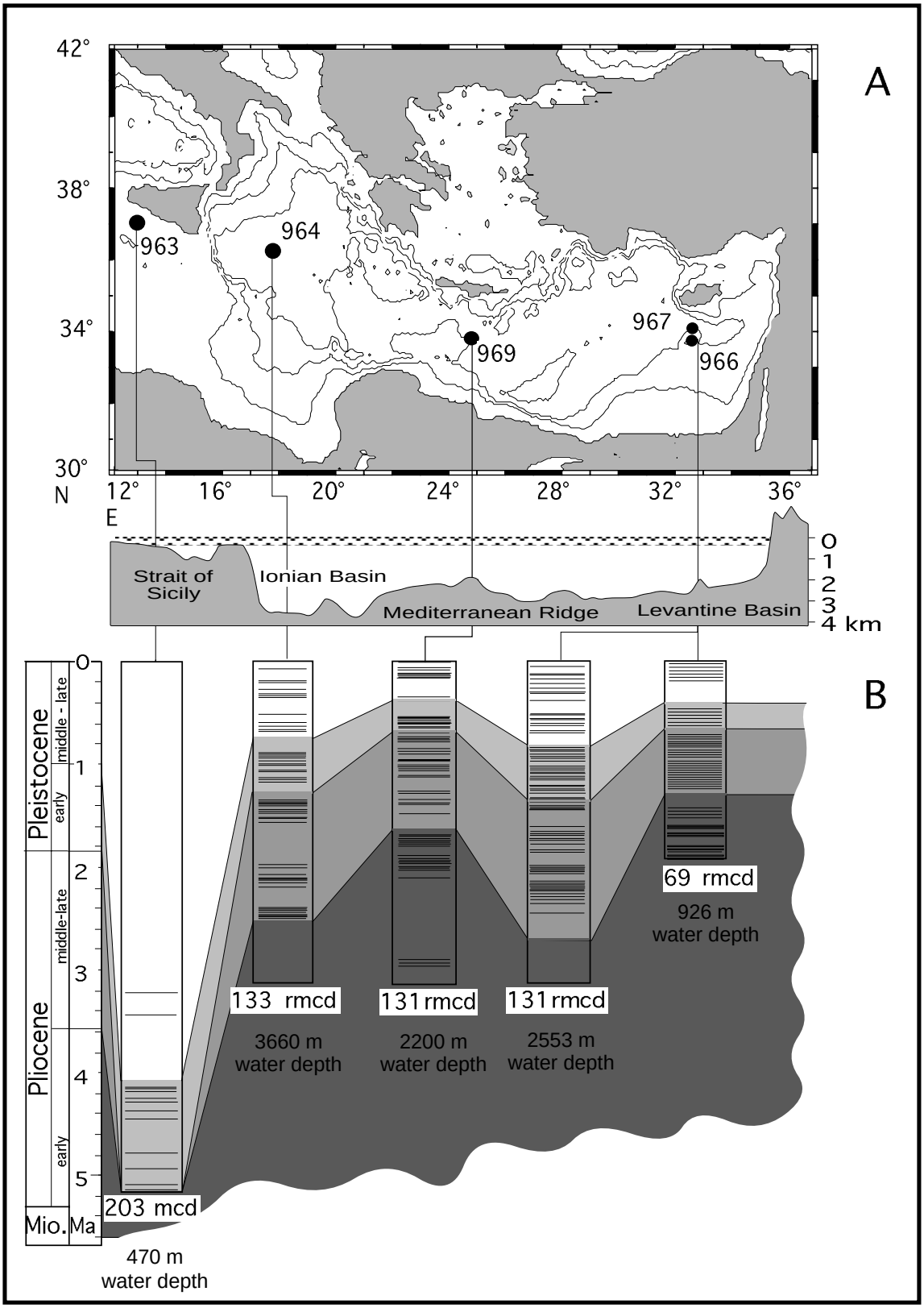

Figure 1. **A.** Locations of Leg 160 paleoceanographic sites. **B.** Preliminary stratigraphy of drilled sites. The bars in each column show the occurrence of sapropels. Abbreviations are defined as follows: rmcd = revised meters composite depth; mcd = shipboard meters composite depth.

138 (Hagelberg et al., 1995), Leg 145 (Rea, Basov, Janecek, Palmer-Julson, et al., 1993), and Leg 154 (Curry, Shackleton, Richter, et al., 1995).

A particular meters below seafloor (mbsf) depth recorded in each hole at any one site obviously does not represent the same stratigraphic depth in those holes (Fig. 2). The mbsf scale is calculated by subtracting the distance between rig floor and water depth from total length of the drill string. This convention does not take into account such variables as ship and drill string motion, deformation as a result of the coring process, changes in hydrostatic pressure between material in situ and that at sea level, shipboard handling techniques, and other factors. In addition, tectonic faulting and diagenetic overprinting are natural causes of between-hole differences in recorded mbsf depths. In light of all these coring and tectonic problems, the construction of high-resolution, centimeter-scale, composite depth sections from interhole correlation is the only way to evaluate the continuity of stratigraphic sequences, especially in the cores recovered during Leg 160.

The history of composite depth section construction has been reviewed in Hagelberg et al. (1995). Composite depth sections were constructed from a variety of high-resolution measurements, including visual or digital color variation, core photographs, magnetic susceptibility, gamma-ray attenuation porosity evaluator (GRAPE) density, and carbonate and biogenic opal contents. During Leg 160, shipboard composite depth sections were constructed for Sites 963, 964, 966, 967, 968, 969, and 973 from color reflectance, GRAPE bulk density, and magnetic susceptibility data (with sampling resolutions varying between 2 and 10 cm) using software provided by Lamont Doherty Earth Observatory (Emeis, Robertson, Richter, et al., 1996). These shipboard composite depth sections were useful in guiding coring operations at each site to ensure that a continuous sedimentary section was recovered. The construction of the shipboard composite depth sections, however, did not correct for the ubiquitous within-core deformation resulting from coring operations, tectonic disturbances such as faulting and slumping, or differences in sedimentation rates (Fig. 2). The postcruise composite depth sections presented be-

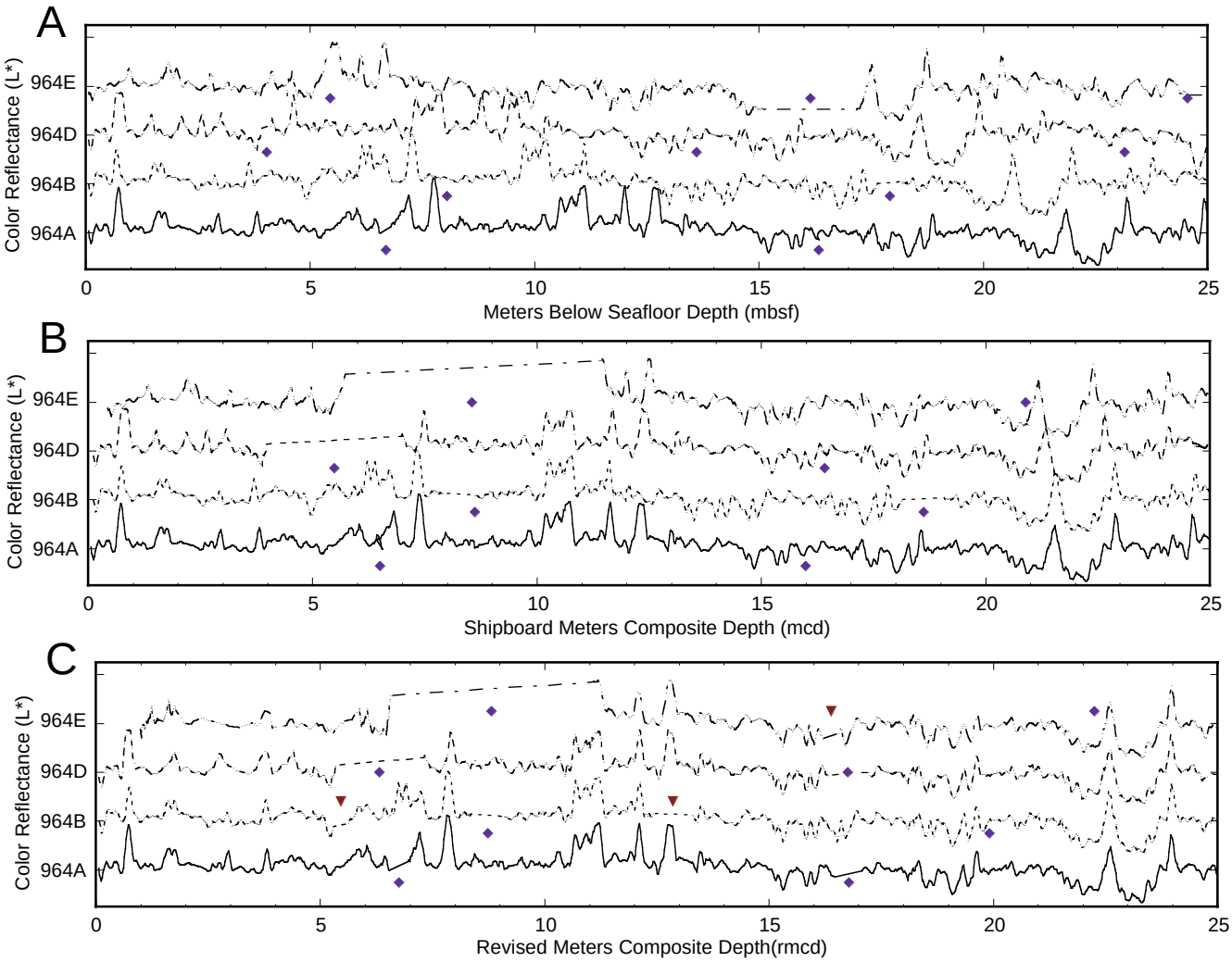

Figure 2. Examples of color reflectance (five-point smoothing on a relative scale) for Holes 969A, 969B, 969D, and 969E showing how the composite procedure aligns coeval intervals between holes: **(A)** mbsf, **(B)** mcd, and **(C)** rmcd. The diamonds show the horizons of coring artifact gaps. The triangles show the horizons of gaps resulting from faulting. The plots in mbsf (A) do not show alignment of stratigraphically coeval horizons. The shipboard mcd (B) corrected for coring artifact gaps, but did not correct effects of natural faulting or stretching and condensing of the sediments within a core. For example, the isochronous horizons around 22 mcd are not aligned properly because the shipboard composite procedure only shifted whole cores. The alignment in rmcd (C) is stratigraphically most accurate because it stretches and squeezes data within a core and accounts for gaps within a core.

low (hereafter referred to as revised composite depth sections and r_composite in figures) were constructed to correct not only artificial (i.e., coring-induced) disturbances, but also tectonic disturbances and natural sedimentological variations (i.e., changes in sedimentation rate) found in the sediment sequences at each site (Fig. 2).

The detailed correlation methods presented below are able to estimate (1) gaps between APC cores and gaps within cores caused by tectonic disturbances, (2) the degree of expansion and stretching of cores, (3) differences of sedimentation rates among holes at a site, and (4) variability of preservation of coeval sapropels. The results are presented as mbsf-revised meters composite depth (rmcd) transfer tables, tie points of interhole correlations, and tables of coring gaps and faults in rmcd. All the data tables, as well as images of cores with correlation lines, are found on CD-ROM (back pocket, this volume).

METHODS

We worked on four sites (Fig. 1), which are located in different tectonic and oceanographic settings and water depths (Site 964: 3660 m water depth in the Ionian Basin; Sites 966 and 967: 926 m and 2553 m water depth on the Eratosthenes Seamount; Site 969: 2200 m water depth on the Mediterranean Ridge). At each of those sites (Fig. 1), multiple APC holes were drilled: four holes at Site 964, five holes at Site 966, and six holes at Sites 967 and 969 (Emeis, Robertson, Richter, et al., 1996)

Correlation Data Sets

The color reflectance data sets collected during Leg 160 provide the best tool for correlation between holes. Variations in the color data provide a good approximation of lithological features in most cores (see "Lithology" section in each site chapter in Emeis, Robertson, Richter, et al., 1996). Other continuous whole-core measurements, such as magnetic susceptibility and GRAPE bulk density, did not produce as high-quality signal variation as the color data from these Mediterranean sediments. These data sets, however, provided useful supplementary information because correlations depending on color data alone sometimes resulted in the misidentification of lithologic features. For example, abrupt decreases in color reflectance can signal the transition to several types of lithologies, including dark silt layers, dark ash layers, pyrite flakes, burrows filled by dark materials, and organic-rich layers. Iteration of the correlation procedure using magnetic susceptibility or GRAPE bulk density generally resolved miscorrelation problems.

Immediately after splitting the cores on the ship, color reflectance data were collected at 2-cm intervals using a handheld Minolta CM-2002 color spectroscope (Emeis, Robertson, Richter, et al., 1996). This instrument measures and calculates the values of the L*a*b* color system, the Munsell color scheme, and percent reflectance (400 to 700 nm in wavelength) for each measurement (Emeis, Robertson, Richter, et al., 1996). The L*a*b* data, in particular the L* value, proved most useful for our postcruise work. The L*a*b* color system is a three-dimensional expression of (1) lightness (high values of L* indicate lighter colors), (2) red and green (positive values of a* indicate red), and (3) yellow and blue (positive values of b* indicate yellow).

After Site 963 (the first site of the leg, in which several measurement errors occurred while developing correct procedures), every split-core section was covered with plastic wrap before spectroscopic analysis. Shipboard scientists carefully smoothed out wrinkles in the wrap and pushed out air bubbles between the wrap and sediment surface without disturbing the sediments. The measuring lens of the Minolta spectroscope was always placed directly on the wrap to avoid measurement errors. Plastic-wrapped, white, standard objects were used for calibration (Emeis, Robertson, Richter, et al., 1996).

Composite Depth Section Construction

To construct revised composite depth sections, it was necessary to determine the length of gaps at the APC core breaks and to correct for the differential stretching and condensing of the sediments within a core. In addition, it was necessary to assess whether these distortions were the result of coring processes or natural variations, such as faulting, slumping, and/or mass flows. These problems required correlation of holes down to the centimeter scale.

The concept of composite section construction is based upon the assumption that adjacent holes penetrate a perfect "layer cake" stratigraphy. In environments where faults, erosion, and/or mass flows are common, this approach is not without problems. Because the thickness of layers and formations varies laterally and disturbances such as faulting and slumping can partially erase (or add to) the sequence, any splicing procedure that does not take into account visual observations from split-core surfaces is prone to error. We therefore used digitized color photographs of each archive core and visual core descriptions (VCDs) to assist in correlating the sediments between holes.

The construction of high-resolution revised composite depth sections for Sites 964, 966, 967, and 969 proceeded as follows (Fig. 3A):

1. The core images were digitized by using the 35-mm color slide of each core and a 35-mm slide digitizer set to 72-dpi resolution. These images were edited into columnar images of sediments in a core with a 50% compression in length.
2. The variations of L* were plotted after correcting for known measurement errors that resulted in spurious data values. Measurement errors, noted and catalogued by the shipboard scientists, included instrument mishandling, measurements made when the lens was not in contact with the sediments, and software errors in core numbering.
3. After combining the digitized image and profiles of color reflectance in one image, visual interhole correlation was carried out (example in Fig. 3B; all images are included as interhole correlation figures on CD-ROM, back pocket, this volume). Color reflectance data provide the quantitative data needed to facilitate correlation among holes, whereas the digitized images provide a visual check on the variations of color reflectance. For example, the images help to determine if a decrease in lightness is caused by a dark sapropel layer, by an ash layer, by a dark silt layer, or by cracks in the section resulting from handling in the shipboard laboratories. The handwritten VCDs were also used to check details of lithologic variation.
4. After completion of the shorebased interhole correlation to a decimeter-scale resolution, revised composite depth sections were generated (e.g., Fig. 3B; Table 1). As much as possible, we used cores from a single hole as the basic "backbone" for the revised composite depth sections, and spliced short sections from other holes into core gaps or areas of disturbed sediment within the "backbone" hole (e.g., Table 1). The results of revised composite depth sections are presented as "r_composite tables" and "r_composite data sets" (on the CD-ROM, back pocket, this volume). The r_composite tables include tie points used to construct the revised composite depth section at each site, and the r_composite data sets include the relationship between mbsf and rmcd for the 2-cm intervals of color reflectance measurements.
5. The rmcd data for each hole were calculated by correlating color reflectance variations (L*) of the revised composite depth sections (determined in the previous step) with those of each individual hole. We used the program "AnalySeries" (Paillard, 1996) to evaluate the degree of stretching and squeezing (to centimeter levels) in the "unknown" curves (the individual hole at a particular site) needed for optimal correlation with the "reference curve" (the revised composite section for the

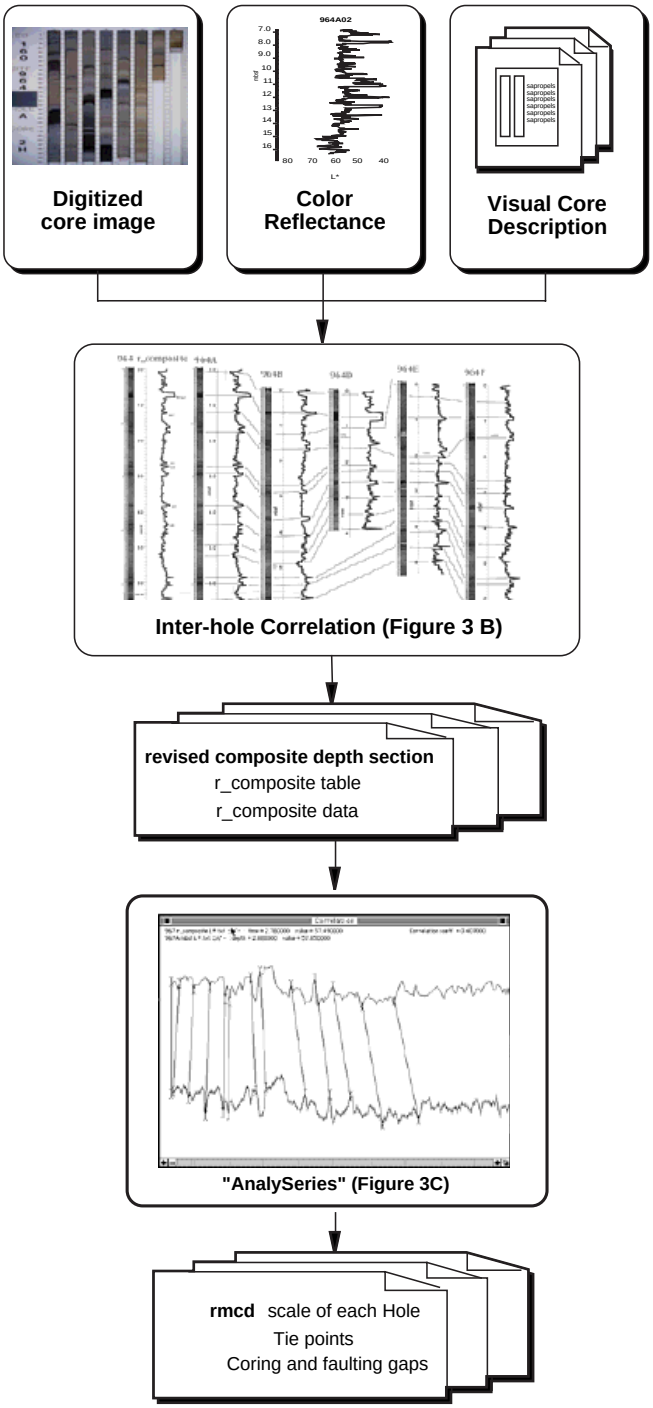

Figure 3. **A.** Scheme of the procedure used to construct the revised composite depth section and rmcd for each hole. (Continued on next page.)

site; Fig. 3C). In the final correlation runs, the correlation coefficients between the two curves were better than 0.90 in most cases.

The tie points used to map each hole to the revised composite depth sections are listed in tie-point tables (on CD-ROM, back pocket, this volume; see Figs. 3 and 4 for examples of final correlation output). These tie points included the abruptly decreasing values of L* representing sapropels, ash layers, dark thin silt layers, light pale layers, reddish silt layers, and bundles of centimeter-scale color-banding. For the sapropels, tie lines were selected at the base of sapropels if the basal boundary showed a sharp contact (Fig. 3C; Site 964, Sapropel 8). If the top boundary of the sapropel was sharp and the bottom boundary was irregular (as a result of bioturbation), tie lines were selected at the top boundaries (Fig. 3B; Site 964, Sapropel 1). If both the boundaries showed sharp features, tie lines were selected at both boundaries of the sapropels (Fig. 3C; Site 964, Sapropels 5 and 7). If both boundaries showed irregular features, tie lines were selected at the middle points of sapropels (Fig. 3C; Site 964, Sapropel 9). These different tie-point procedures resulted in slight differences of rmcd for coeval sapropels at the sites.

6. Gaps between cores and gaps resulting from tectonic disturbances were estimated by hiatuses present in rmcd (Figs. 4–7; e.g., Tables 2, 3).The natural faults were initially identified on the digitized core images and from VCDs, and then were confirmed by comparing sediment sequences above and below faults with other sequences recovered from other holes at the site.

Approximately 90% of the sedimentary sequence was recovered from any single hole drilled during Leg 160 (e.g., Table 2). The composite depth scale is approximately 10%–20% longer than the mbsf scale for Leg 160, as it was in previous legs (Shackleton et al., 1990; deMenocal et al., 1991; Murray and Prell, 1991; Farrell and Janecek, 1991; Hagelberg et al., 1995). The rmcd of each hole is calculated by stretching and condensing an unknown curve (the L* data from each hole) to fit to the reference curve (the L* data of the revised composite depth section). The results of this procedure thus do not represent "true" depth below seafloor. Our aim was to arrange the coeval layers and sequences in multiple holes at the same depth scale and to then make a continuous revised composite depth section at each site from multiple holes. This revised depth scale allows investigators the best possible starting point for further high-resolution stratigraphic and paleoceanographic studies.

RESULTS AND DISCUSSION

Site 964

The sedimentary sequences recovered from Site 964 display abundant color variation and include more natural faults, slumping, and decimeter- to meter-scale turbidites than the other sites we studied. The sediments recovered at Site 964 primarily consist of light-colored (brownish to greenish) clayey nannofossil ooze, nannofossil ooze, and nannofossil clay interspersed with organic-rich, dark layers (sapropels), and numerous ash layers. The nannofossil ooze is generally pale, commonly foraminifer-bearing, and has high L* values. The clayey nannofossil ooze and nannofossil clay lithologies vary between light and dark colors. The alternation of these oozes and clays commonly shows as centimeter- to decimeter-scale color banding on the split-core face. Light reddish color intervals are also present in each hole and aid in establishing correlative horizons among the holes.

The most difficult lithologies to correlate were the brownish, yellowish brown, and dark gray layers. These layers are nannofossil clay, clayey nannofossil ooze, ash layers, and the so-called "ghost" sapropels. In our study, we use the term "ghost" sapropels for heavily bioturbated, oxidized, or "burnt-out" sapropels. These layers were described as "oxidized" sapropels, "burnt out" sapropels, "eaten" sapropels, "proto" sapropels," "pale" sapropels or "sapropelic" in the shipboard VCDs (Emeis, Robertson, Richter, et al., 1996).

We constructed the continuous revised composite depth sections from five holes (Holes 964A, 964B, 964C, 964D, and 964E; Table 1,

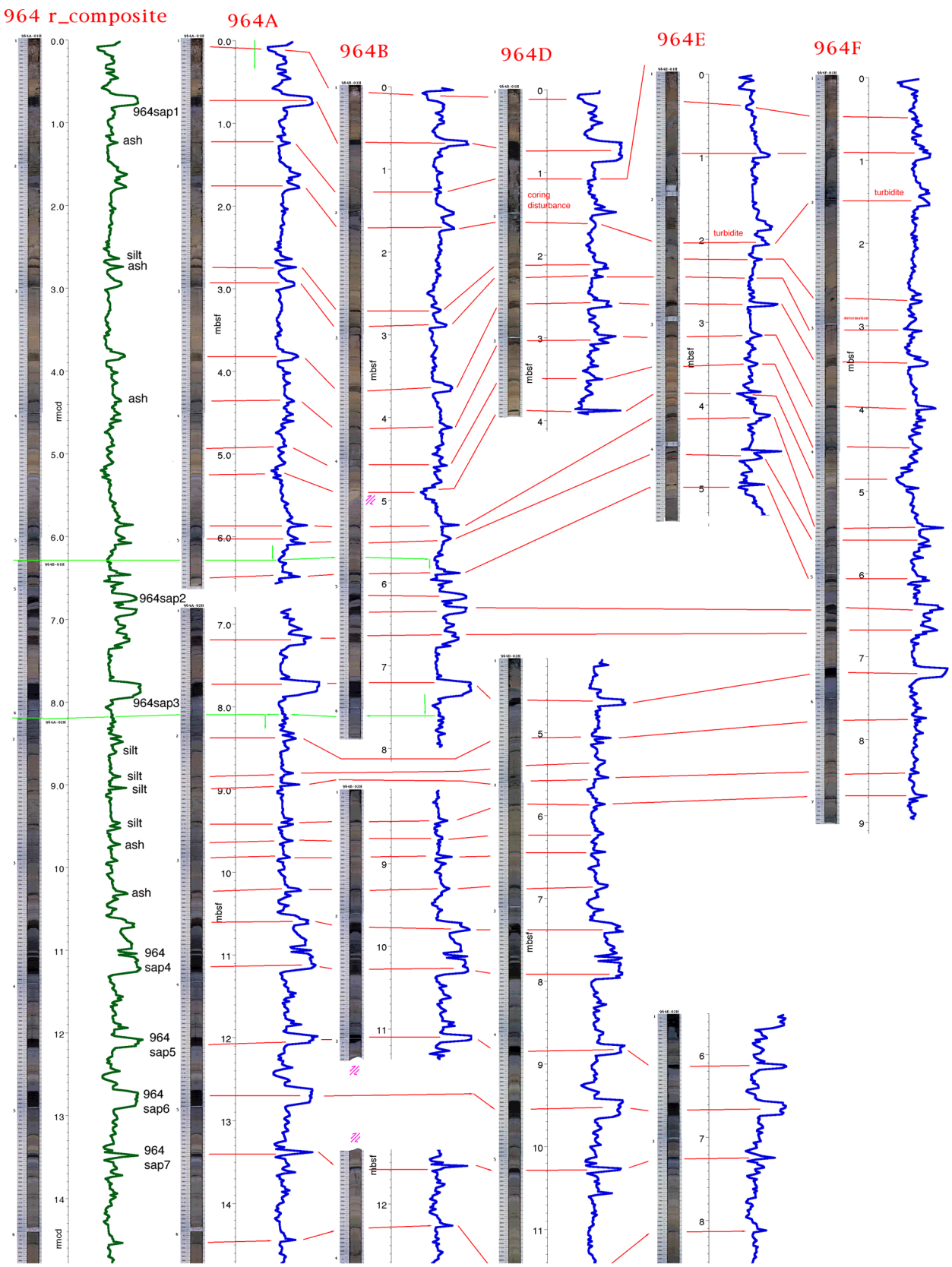

Figure 3 (continued). **B.** Example of initial visual interhole correlation at Site 964 using L* color data. Tie lines show coeval horizons. Fault intervals (in Sections 160-964B-2H-3, 964D-3H-6, and 964E-2H-3) and repeated sequences (in Sections 160-964B-1H, 964E-3H-1, and 964E-3H-2) are clarified by interhole correlation. (Continued on next page.)

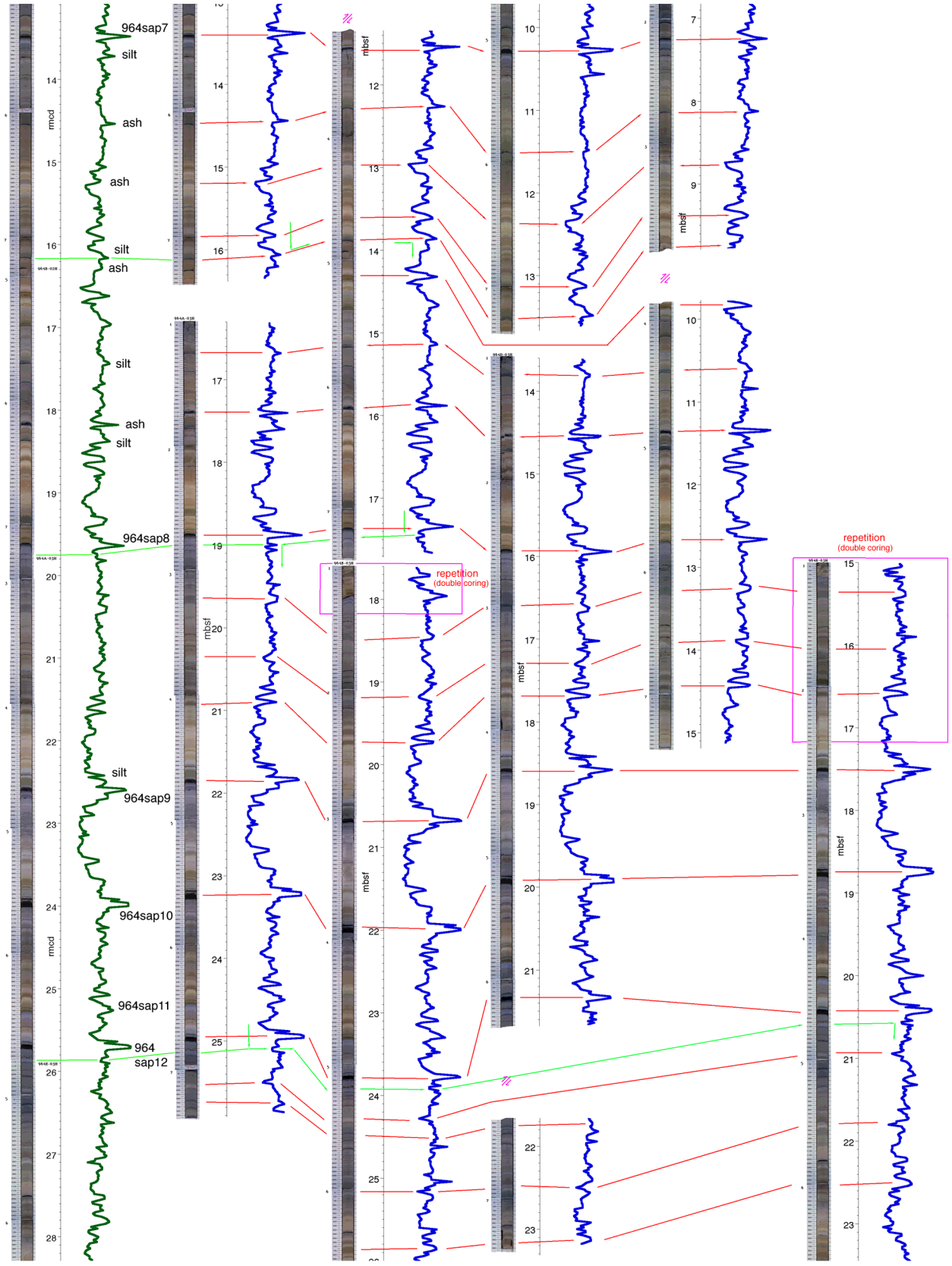

Figure 3B (continued).

Fig. 4; all rmcd tie-point data on CD-ROM [back pocket, this volume] associated with this volume). A total of 59 individual sapropels can be identified in the composite section. Although the sedimentary sections from the five holes have many similar features, the composite depth section consists of relatively short intervals from all the holes because of the extensive disturbance by faulting and slumping that affected each hole. The total length of the rmcd section is 133 rmcd, 25 m longer than the mbsf sequence. The total sediment recovery for each hole (i.e., the ratio of the recovery of the sediments from each hole in comparison to the entire composite sedimentary sequence) is, on average, 88.5%; 93% in Hole 964A, 86% Hole 964B, and 84% in Hole 964D (Table 2).

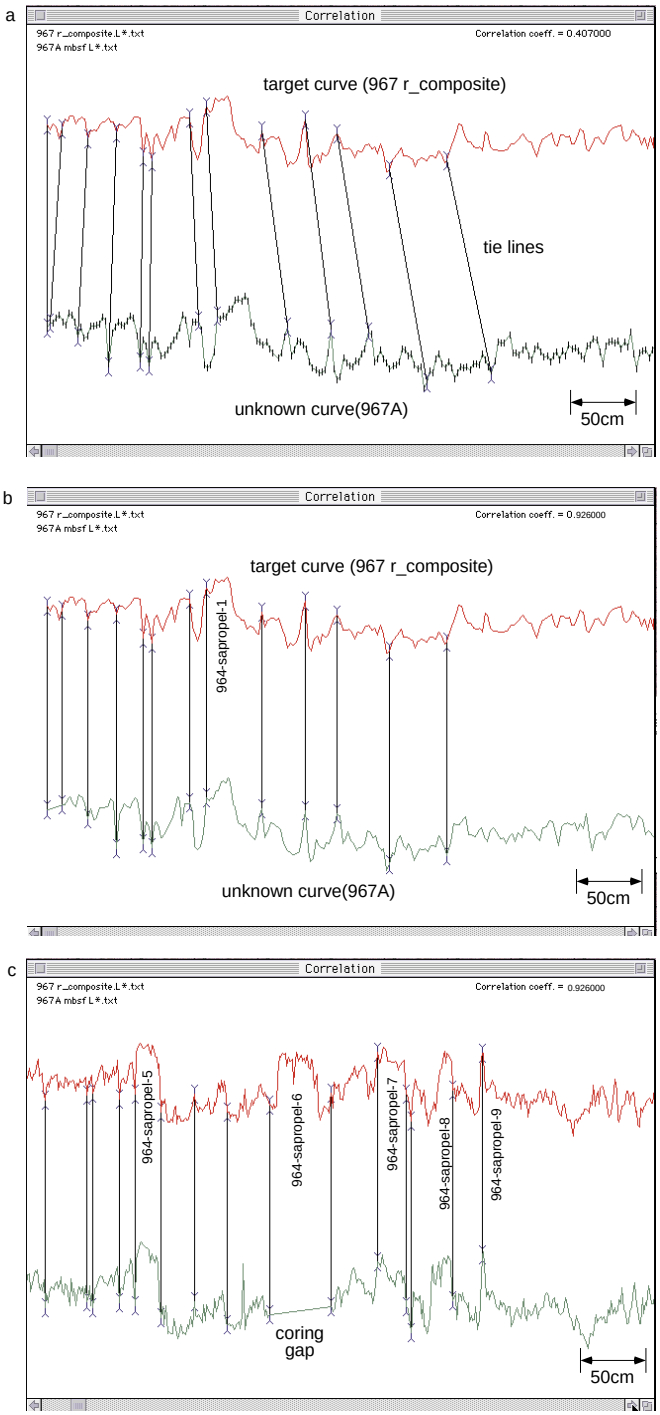

Figure 3 (continued). **C.** Examples of AnalySeries data windows: **(a)** before tuning, and **(b)** and **(c)**: after tuning. Tie lines (a) are shown between the target curve (967 r_composite or revised composite depth section) and an unknown depth curve (Hole 967A). The rmcd of Hole 967A is calculated by linear tuning to the target curve. See "Composite Depth Section Construction" above for a description of the tie-line strategy for different sapropel types.

The mbsf-rmcd conversion table for Hole 964C was constructed only for Cores 160-964C-6H through 10H, because color reflectance was not collected for the other Hole 964C cores, and GRAPE bulk density and magnetic susceptibility data could not provide unambiguous correlations for the remainder of the cores from that hole. Similarly, the mbsf-rmcd conversion table for Hole 964F was constructed only for Core 160-964F-1H. Although shipboard color reflectance generally was measured at 2-cm intervals, some intervals were measured using a sample spacing of 5 cm. These intervals (from Section 160-964B-11H-2, 110 cm, to the bottom of Section 160-964B-11H-6; from Section 160-964C-9H-3, 120 cm, to Section 160-964C-9H-4, 150 cm; from Section 160-964E-4H-1, 0 cm, to Section 160-964E-4H-1-150 cm; and the basal 75 cm in Core 160-964D-12H) may thus have a lower correlation precision than the other intervals.

The rmcd data show that several intervals were cored twice. The duplicate intervals always occur at core tops (from Section 160-964B-3H-1, 0 cm, to Section 160-964B-3H-1, 57 cm; and from Section 160-964E-3H-1, 0 cm, to Section 160-964E-3H-2, 66 cm), suggesting that the repeat intervals are the result a new core recoring material recovered from the previous core, rather than the result of introduction of duplicate material by a reverse fault or slumping.

The gaps between cores are, on average, 1.31 m at Site 964 (Table 2; Fig. 4), with the largest gap (7.78 m) occurring between Cores 160-964A-7H and 8H. This large gap is not an artifact of the coring process, but represents material missing as a result of natural faulting. The largest nontectonic gap between cores (6.47 m) occurs between Cores 160-964D-10H and 11H, with other large coring artifact gaps found between Cores 160-964B-6H and 7H (3.26 m), Cores 160-964B-7H and 8H (2.80 m), Cores 160-964D-1H and 2H (1.93 m), Cores 160-964-10H and 11H (3.52 m), and Cores 160-964E-1H and 2H (4.48 m).

The gaps within cores resulting from faulting and erosion of turbidites that were taken into account in construction of the rmcd table are listed in Table 3 and shown in Figure 4. As the discontinuity surface of faulting and erosion generally is not horizontal, intervals where they occur range in length from centimeter- to decimeter-scale. The extent of gaps in the sequences could be estimated from distinct jumps in rmcd on the composite reflectance curves for each hole. The gaps represent "primary structures," not coring disturbances, because the sequences above and below the fault planes could be correlated with sequences recovered from other holes. Average gaps created by tectonic disturbances at Site 964 are 1.25 m in length and range from 6 cm to 7.78 m (both in Core 160-969A-8H). Other significant faulting gaps occur in Sections 160-964A-6H-4 (1.52 m), 160-964B-4H-2 (2.88 m), 160-964C-9H-5 (1.84 m), 160-964C-10H-2 (2.58 m), 160-964D-5H-2 (2.30 m), and 160-964E-5H-5 (1.64 m). The gaps in Sections 160-964D-7H-6 (2.08 m), 160-964D-9H-1 (0.84 m), and 160-964E-4H-2 (1.02 m) occur at the base of turbidites.

The sedimentary sequence at Site 964 includes four significant turbidites: from 52.50 to 53.96 rmcd, 70.68 to 72.86 rmcd, 92.27 to 94.76 rmcd, and 107.12 to 108.26 rmcd. In the interhole correlation, these turbidites were treated as being the same thickness in rmcd, although the facies and thickness of each turbidite differ from hole to hole. In addition, the intervals from Section 160-964E-1H-1, 0 cm, to Section 160-964E-1H-2, 58 cm, and from Section 9160-64F-1H-1, 0 cm, to Section 160-964F-1H-2, 5 cm, also include turbidites. The interhole correlation shows that the core tops of Holes 964E and 964F

Table 1. Revised composite depth section of Site 964.

Leg	Site	Hole	Core	Type	Section	Top	Bottom	Depth (mbsf)	tie	Leg	Site	Hole	Core	Type	Section	Top	Bottom	Depth (mbsf)	Depth (rmcd)
160	964	A	1	H	1	2.0	2.1	0.02											0.02
160	964	A	1	H	5	28.0	28.1	6.28	→	160	964	B	1	H	4	120.0	120.1	5.70	6.28
160	964	A	2	H	1	128.0	128.1	8.08	←	160	964	B	1	H	6	10.0	10.1	7.60	8.18
160	964	A	2	H	7	26.0	26.1	16.06	→	160	964	B	2	H	4	126.0	126.1	13.86	16.16
160	964	A	3	H	2	120.0	120.1	19.00	←	160	964	B	2	H	7	36.0	36.1	17.46	19.76
160	964	A	3	H	6	130.0	130.1	25.10	→	160	964	E	3	H	4	106.0	106.1	20.56	25.86
160	964	D	4	H	1	62.0	62.1	23.72	←	160	964	E	3	H	6	136.0	136.1	23.86	29.16
160	964	D	4	H	6	134.0	134.1	31.94	→	160	964	B	4	H	3	72.0	72.1	30.82	37.38
160	964	A	5	H	2	34.0	34.1	37.14	←	160	964	B	4	H	6	130.0	130.1	35.90	42.46
160	964	A	5	H	5	20.0	20.1	41.50	→	160	964	B	5	H	2	126.0	126.1	39.36	46.82
160	964	A	6	H	1	124.0	124.1	46.04	←	160	964	B	5	H	6	78.0	78.1	44.88	52.34
160	964	A	6	H	3	90.0	90.1	48.70	→	160	964	D	6	H	2	118.0	118.1	44.78	55.00
160	964	B	6	H	5	88.0	88.1	52.98	←	160	964	D	6	H	7	24.0	24.1	51.34	61.56
160	964	B	6	H	6	122.0	122.1	54.82	→	160	964	D	7	H	1	56.0	56.1	52.16	63.40
160	964	B	7	H	2	44.0	44.1	57.54	←	160	964	D	7	H	5	42.0	42.1	58.02	69.26
160	964	B	7	H	4	104.0	104.1	61.14	→	160	964	C	7	H	4	64.0	64.1	57.74	72.86
160	964	D	8	H	1	48.0	48.1	61.58	←	160	964	C	7	H	7	38.0	38.1	61.98	77.10
160	964	D	8	H	7	34.0	34.1	70.44	→	160	964	B	8	H	4	144.0	144.1	71.04	85.96
160	964	C	9	H	1	60.0	60.1	72.20	←	160	964	B	8	H	6	140.0	140.1	74.00	88.92
160	964	C	9	H	5	62.0	62.1	78.22	→	160	964	D	9	H	5	44.0	44.1	77.04	94.94
160	964	A	9	H	1	132.0	132.1	74.62	←	160	964	D	9	H	6	10.0	10.1	78.20	96.10
160	964	A	9	H	6	140.0	140.1	82.20	→	160	964	E	6	H	5	74.0	74.1	82.74	103.68
160	964	A	10	H	1	62.0	62.1	83.42	←	160	964	E	6	H	7	36.0	36.1	85.36	106.30
160	964	A	10	H	7	24.0	24.1	92.04	→	160	964	B	11	H	1	10.0	10.1	93.70	114.92
160	964	A	11	H	1	142.0	142.1	93.72	←	160	964	B	11	H	2	98.0	98.1	96.08	117.30
160	964	A	11	H	6	146.0	146.1	101.08	→	160	964	D	12	H	1	95.0	95.1	100.05	124.84
										160	964	D	12	H	7	20.0	20.1	108.30	133.09

are missing, possibly the result of erosion or disturbance by the drill pipe before the core was taken.

Site 966

As at other Leg 160 sites, the sediments recovered at Site 966 are dominated by nannofossil ooze and clayey nannofossil ooze. The color variation in nannofossil oozes and clays at Site 966, however, is less than that seen at other Leg 160 sites. The sapropels at this site are heavily bioturbated and exhibit a remarkable variability in color and thickness. Significant interhole differences in sapropel patterns are evident; coeval sapropels very commonly are ghost sapropels in some holes, whereas they are well preserved in other holes. Compared with Site 964, the sediment record of Site 966 is not disturbed by tectonic processes (natural faults and slumps), and the correlation procedure was very straightforward.

The revised composite section was constructed from Holes 966B and 966D (Table 4; Fig. 5; rmcd and tie-point data on CD-ROM [back pocket, this volume]). Comparison of the sapropel sequences and other lithologic features between holes at Site 966 shows that Hole 966A is more condensed relative to the other holes. The total rmcd for Hole 966A is 69.12 rmcd, only 4.22 m longer than the mbsf value. The total recovery of each hole compared to the revised composite sequence is 93% on average, with the recovered sediments at Hole 966A representing only 85% of the total revised composite sequence (Table 5). A total of 64 sapropels and 24 ghost sapropels were identified in the revised composite section.

The deeper sequences at Site 966 exhibit considerable hole-to-hole variability. For example, two very similar thick sapropels occur between 66.5 and 67 rmcd in Cores 160-966A-7H and 160-966C-7H. These sapropels can be correlated with sapropels in Cores 160-966B-7H and 966D-7H that have similar lithological features, but are much thinner in extent. The difference in the sapropel thickness may be attributed to changing depositional conditions resulting from distinct bathymetric differences between the holes at the time of deposition.

Coring gaps range from 3 cm to 1.86 m in rmcd (Table 5). Significant gaps (>1 m in rmcd) occur between all of the successive cores From Hole 966A, between Cores 160-966D-2H and 3H, and between Cores 160-966D-3H and 4H.

Site 967

The sediments recovered at Site 967 primarily consist of bioturbated nannofossil oozes, nannofossil clays, and sapropels. The revised composite depth section was constructed from four holes: Holes 967A, 967B, 967C, and 967D (Table 6; Fig. 6; all rmcd and tie-

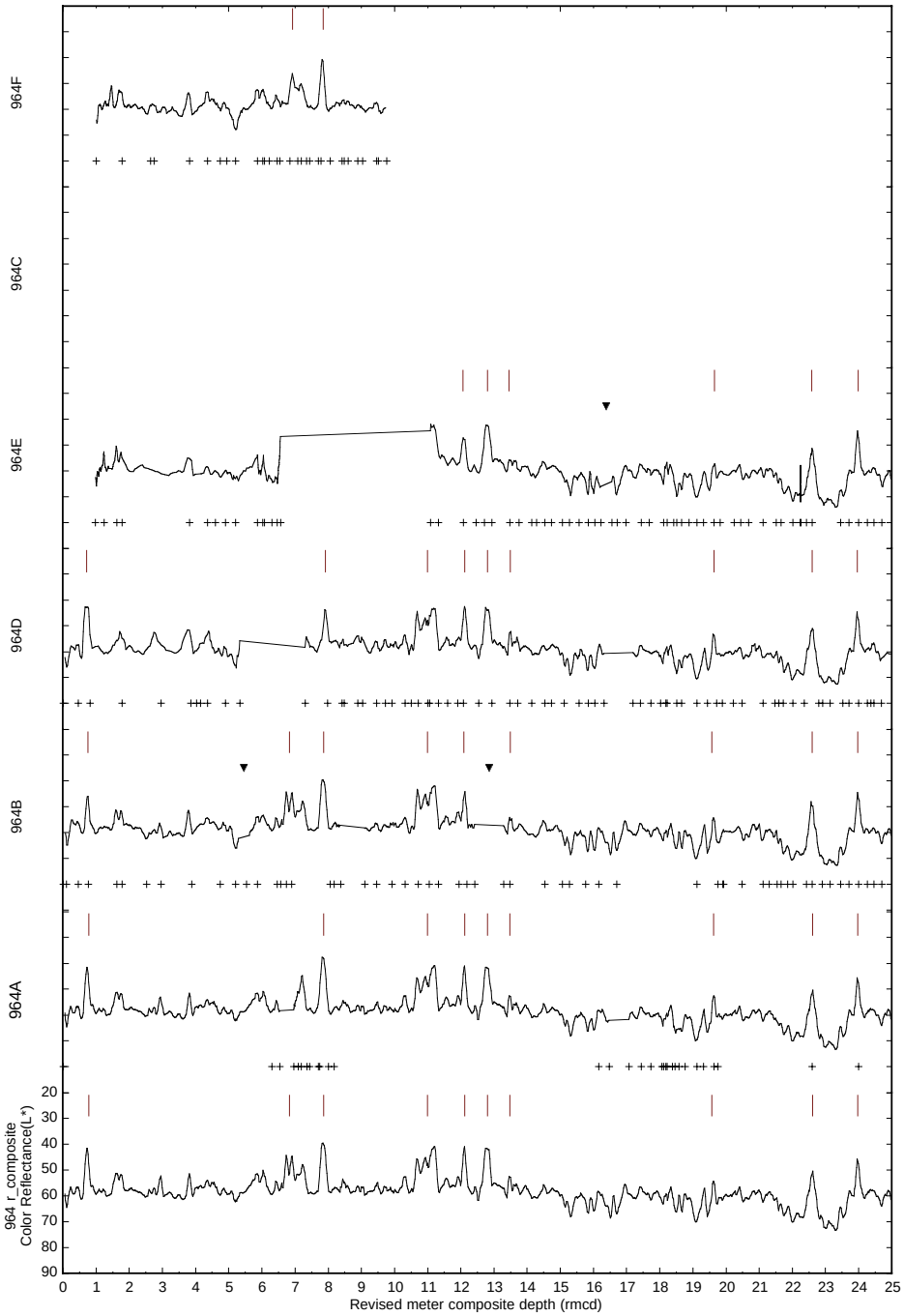

Figure 4. **A.** Plots of L* color data on an expanded scale (0–25 rmcd) showing the revised composite depth section for Site 964 (lowermost curve) and the L* data, in rmcd, for all the holes at Site 964. The bars above the curves show the occurrence of sapropels and ghost sapropels. The crosses below the curves show tie points between the revised composite depth section and curve of each hole. The triangles above each curve show gaps at the fault horizons. The straight lines in each curve show coring-artifact gaps. (Continued on next page.)

point data included in tables on CD-ROM, back pocket, this volume). Eighty individual sapropels and 10 ghost sapropels were recognized in the composite.

The sedimentary section at Site 967 was relatively undisturbed by tectonic processes except for one interval. A slumped interval occurs from 53.08 to 67.02 rmcd in all the deeper holes at the site (from Section 160-967A-6H-5, 110 cm, to Section 160-967A-7H-4, 60 cm, from Section 160-967B-7H-1, 114 cm, to Section 160-967B-7H-5, 63 cm, and from Section 160-967C-6H-4, 54 cm, to Section 160-967C-6H-5, 34 cm). The sequences from these holes are heavily disturbed over the interval from 57.28 to 64.5 rmcd. The sediments from 60.33 to 64.30 rmcd in Hole 967C are missing. Although all holes in these intervals were disturbed to some extent by slumping, we used sequences from Hole 967B for the upper part and from Hole 967C for the lower part in this slumped unit to construct the composite section. Both of these intervals appear to be less stratigraphically disturbed than equivalent intervals from Hole 967A.

On average, 92% of the sediments in the revised composite depth section was recovered from the individual holes: 91% at Hole 969A, 92% at Hole 969B, and 94% at Hole 967C (Table 7). Gaps between

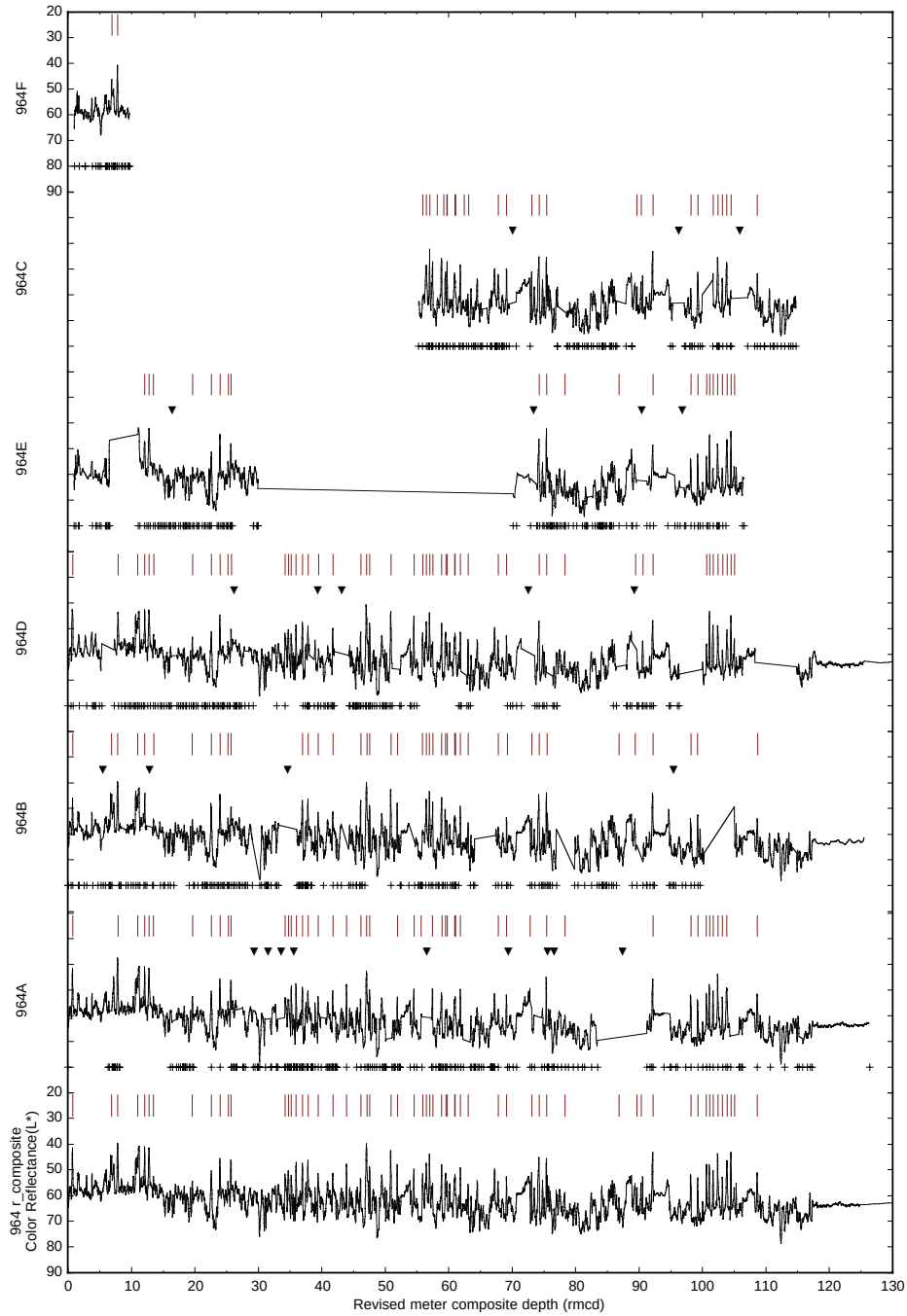

Figure 4 (continued). **B.** Plots of L* color data (0–130 rmcd) showing the revised composite depth section for Site 964 (lowermost curve) and the L* data, in rmcd, for all the holes at Site 964. The bars above the curves show the occurrence of sapropels and ghost sapropels. The crosses below the curves show tie points between the revised composite depth section and curve of each hole. The triangles above each curve show gaps at the fault horizons. The straight lines in each curve show coring-artifact gaps.

cores average 80 cm at this site (the least at any of the sites we examined), and gaps >1 m in length occur in all holes. The largest coring gap occurs between Cores 160-969A-12H and 13H (3.87 m).

Site 969

The sediments recovered from holes drilled at Site 969 show remarkable differences in sedimentation rate, degree of sapropel preservation, and inclination of layers, which makes interhole correlation very difficult at this site. The cores from Holes 969A, 969B, 969D, and 969E were used to construct a nearly continuous sedimentary sequence for the revised composite section (Tables 8–10; Fig. 7; all of the rmcd and tie-point data are included on CD-ROM, back pocket, this volume). Two intervals, however, could not be covered by undisturbed sequences from other holes; the fault interval at Sections 160-969A-10H-5, 70 cm, 160-969B-10H-2, 20 cm, and 160-969D-3H-4, 105 cm, and a gap between Cores 160-969A-10H and 11H. These intervals are treated as continuous in the revised composite depth section, even though some material is probably missing. The revised composite depth section is 131.15 m long, ~30 m longer than any of

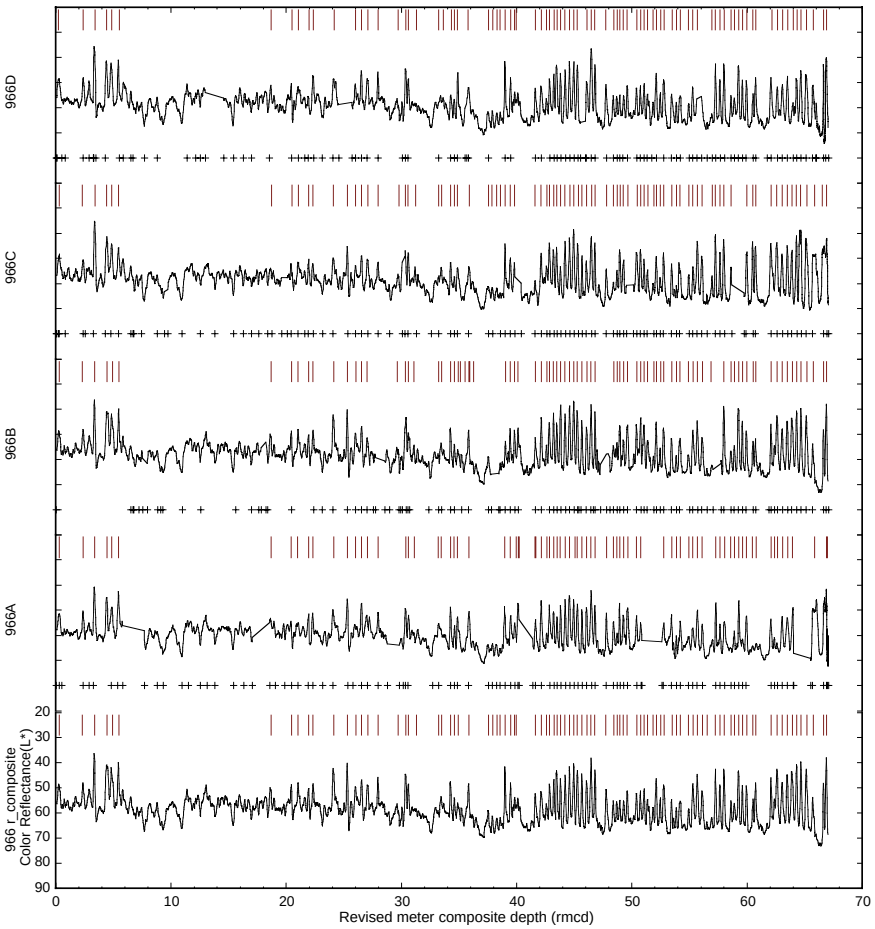

Figure 5. Plots of L* color data (0–70 rmcd) showing the revised composite depth section for Site 966 (lowermost curve) and the L* data, in rmcd, for all the holes at Site 966. The bars above the curves show the occurrence of sapropels and ghost sapropels. The crosses below the curves show tie points between the revised composite depth section and curve of each hole. The straight lines in each curve show coring-artifact gaps.

the mbsf sequences from the individual holes. This is the largest differences between rmcd and mbsf of any of the sites studied. The ratios of recovered sedimentary sections of each hole compared with the composite is 92% in Hole 969A, 86% in Hole 969B, 92% in Hole 969C, and 86% in Hole 969D. After construction of the revised composite section, we found 83 sapropels and 26 ghost sapropels, including the oldest sapropel bundles of all the drilled sites.

Although Hole 969D was drilled only about 100 m from any of the other holes, the sedimentary sequence at Hole 969D is quite different in that it has a higher sedimentation rate, greater degree of inclination of layers, and more sapropels combined with better sapropel preservation (sapropels present in the Hole 969D section are recognized only as ghost sapropels in Holes 969A, 969B, and 969E). Much of the section from Hole 969D (Cores 160-969D-5H through 9H, and 13H) was used to construct the revised composite depth section (Table 8). Hole 969D has a higher sedimentation rate than the other holes, thus Holes 969A, 969B, and 969E have relatively expanded rmcd scales (refer to the distortion column in Table 9).

Sedimentary layers in Section 160-969D-5H-2 to Core 160-969D-13H have much steeper inclinations than similar intervals in the other holes, which could explain the expanded section at Hole 969D. The mean values of apparent dips in cores were measured on digitized core images (Table 11). To determine the "true" thickness of these inclined sequences from Hole 969D for the revised composite depth section, we used the following equation:

"True" thickness = cosine (angle of apparent dip)
× apparent thickness.

The dip angles were taken from the digitized images of split cores, and thus the measured angles only approximate the actual dips. This calculation, however, is sufficient for the purposes of composite construction. Unfortunately, the observed differences in thickness between the section recovered from Hole 969D and those from other holes cannot be explained by bedding inclination alone because the sedimentary section recovered from Hole 969D remains thicker even after application of tilt corrections. The difference in sediment thickness first occurs in Section 969D-4H-3 (at the same horizon as in Sections 160-969A-3H-6, 160-969B-4H-3, and 160-969C-4H-1), however, the inclined sequence begins at a deeper level in Hole 969D (Section 160-969D-5H-2). In addition, the difference in sediment thickness between Hole 969D and that from other holes is greater in the upper part of the tilted sequence where inclinations in Hole 969D are low (Table 11). Moreover, the difference in sediment thickness between holes is not large where the inclination of layers in Hole 969D is relatively high in the deeper part of that hole (below Section

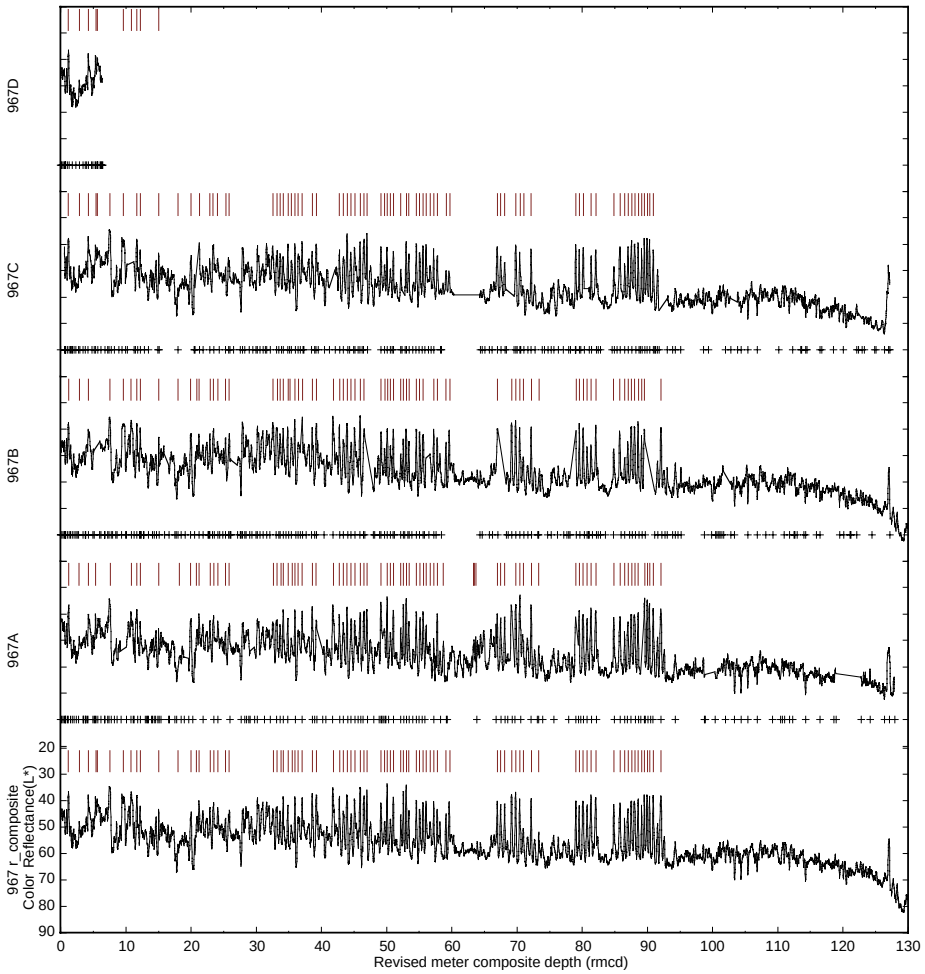

Figure 6. Plots of L* color data (0–130 rmcd) showing the revised composite depth section for Site 967 (lowermost curve) and the L* data, in rmcd, for all the holes at Site 967. The bars above the curves show the occurrence of sapropels and ghost sapropels. The crosses below the curves show tie points between the revised composite depth section and curve of each hole. The straight lines in each curve show coring-artifact gaps.

160-969D-11H-6, which correlates with Sections 160-969A-8H-6, 160-969B-9H-1, and 160-969E-8H-5). The reason behind the expanded nature of Hole 969D remains problematic.

The following intervals are not included in rmcd data sets because of coring-induced disturbances: (1) flow-in intervals in intervals 160-969A-11H-6 and 11H-7; 160-969B-10H-4 through 10H-7; 160-969D-10H-6, 10H-7, 12H-4, 35–150 cm, 12H-5, and 12H-6; and (2) deformed intervals in Sections 160-969B-11H-1 through 11H-4. In addition, the rmcd for the Core 160-969F-2H was calculated because color reflectance data was not collected for that core, and GRAPE bulk density and magnetic susceptibility data did not provide unambiguous correlations.

A repeated interval occurs in Section 160-969B-2H-1, from 0 to 20 cm. This interval was deleted from the rmcd data. As at Site 964, the duplicate intervals appear at the top of a core, which suggests that the extra material is a result of the new core recoring the same interval as recovered at the base of the previous core, and not the result of tectonic emplacement by a reverse fault or slumping.

Coring gaps >1 m occur in all holes (Table 9). Large gaps were found between Cores 160-969B-2H and 3H (3.71 m), Cores 160-969B-5H and 6H (2.08 m), Cores 160-969D-12H and 13H (2.87 m), Cores 160-969E-2H and 3H (3.43 m), Cores 160-969E-5H and 6H (2.10 m), and Cores 160-969E-8H and 9H (2.88 m).

Significant gaps (some >2 m) resulting from natural faults also occurred in all of the holes (Table 10; Fig. 7). The largest gap is found in Section160-969E-11H-3 (5.32 m). Stratigraphic gaps caused by natural faulting are commonly much larger than coring artifact gaps at Site 969.

SUMMARY

We have developed revised composite depth sections by combining digitized color images of split cores, VCDs from shipboard operations, and color reflectance measurements with a 2-cm sampling resolution. These new composite data sets use correlation intervals of a few centimeters instead of the 1-to 10-m intervals used in the shipboard composite construction and take into account differential stretching and squeezing within a core. These new composite data sets correct depth differences between holes caused by complicated tectonic regimes and coring artifacts that resulted in attenuated and incomplete sections. The detailed sequences enable us to correlate not only sapropels, but also other lithofacies, such as pale nannofossil

oozes, reddish oozes, dark clays, and ash layers. As many as 83 individual sapropels are recognized in the revised composite depth sections.

The revised composite sections show that APC coring on the *JOIDES Resolution* typically results in gaps on the order of 1 m in length between cores, with some gaps as large as 8 m. Gap length ranges from an average of 0.80 m in length at Site 967 to an average of 1.31 m at Site 964. The most tectonically disturbed sites (Sites 964 and 969) appear to have the largest gaps between cores. At the sites examined in this study, gaps within cores and between cores also resulted from material lost by faulting and slumping. These "tectonic" gaps are similar in magnitude to coring artifact gaps (average 1–2 m), with some as large as 8 m.

Comparison of the revised composite section with the individual holes at each studied Leg 160 site reveals that, on average, 90% of the sedimentary section is recovered in any one "continuous" APC hole (i.e., a hole in which core recovery was at least 100% according to ODP convention) with a range from 84% to 94%.

The revised composite depth sections in this study can be used as starting points for the development of high-resolution time scales and

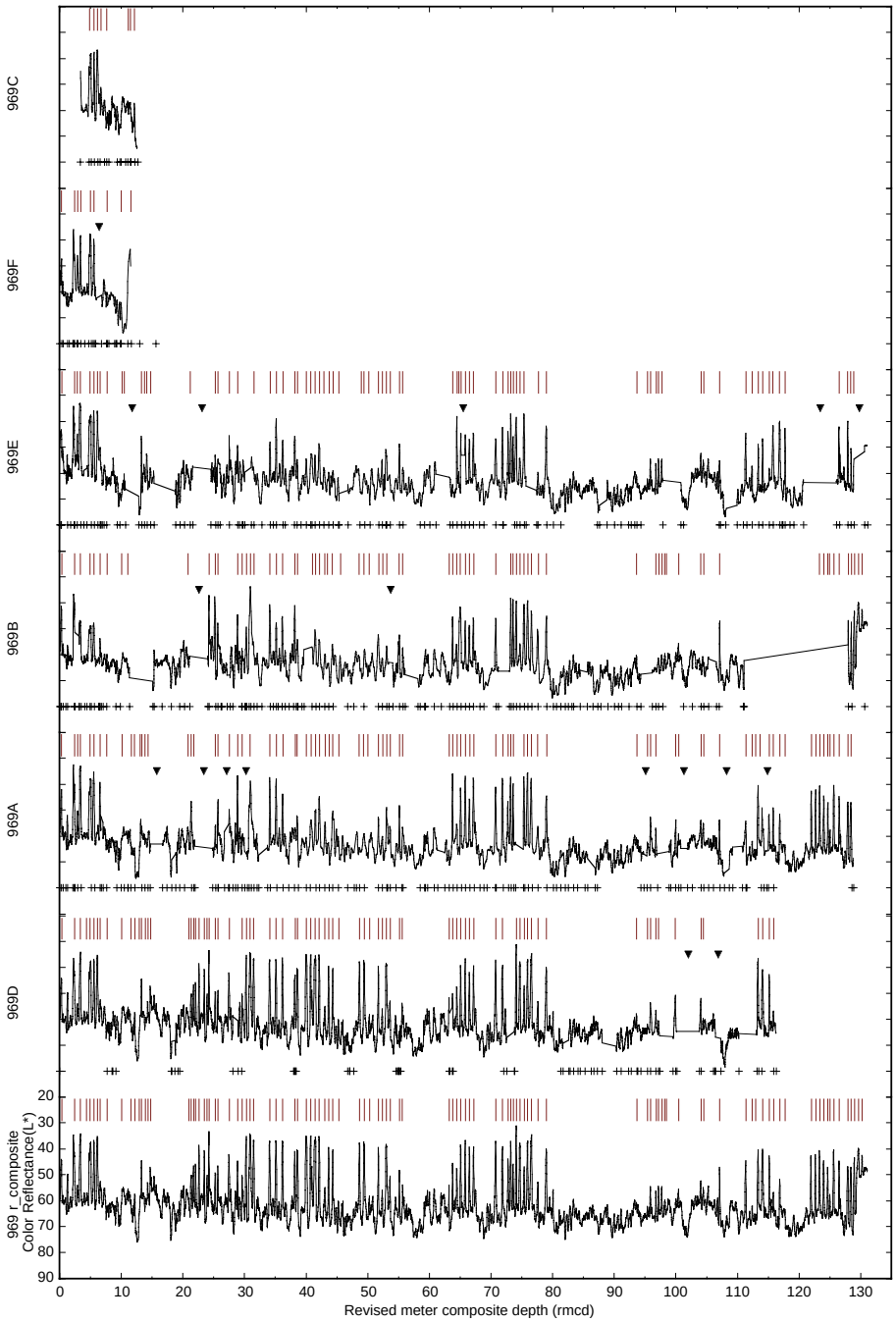

Figure 7. Plots of L* color data (0–130 rmcd) showing the revised composite depth section for Site 969 (lowermost curve) and the L* data, in rmcd, for all the holes at Site 969. The bar above the curves show the occurrence of sapropels and ghost sapropels. The crosses below the curves show tie points between the revised composite depth section and curve of each hole. The triangles above each curve show gaps at the fault horizons. The straight lines in each curve show coring-artifact gaps.

paleoceanographic time series in the Mediterranean. This technique, if carefully applied for the given conditions, can successfully produce preliminary site-to-site correlations that will give value to and impetus for future work.

ACKNOWLEDGMENTS

The color reflectance data and VCDs were the basis of the present study. We thank all shipboard sedimentologists for their detailed descriptions and thank all scientists and technicians involved with color reflectance measurements. L. Lourens provided a valuable comment concerning the slumped intervals in the revised composite depth section at Site 967. T. Sakamoto was funded by the Japanese Society of the Promotion of Science Fellowship for Research at Centers of Excellence Abroad. Funding for T. Janecek was provided by the JOIDES U.S. Science Support program. K.-C. Emeis acknowledges funding under contract DFG EM-37/4, IOW contribution No. 244.

REFERENCES

Alexandrovich, J.M., and Hays, J.D., 1989. High-resolution stratigraphic correlation of ODP Leg 111 Holes 677A and 677B and DSDP Leg 69 Hole 504. *In* Becker, K., Sakai, H., et al., *Proc. ODP, Sci. Results*, 111: College Station, TX (Ocean Drilling Program), 263–276.

Curry, W.B., Shackleton, N.J., Richter, C., et al., 1995. *Proc. ODP, Init. Repts.*, 154: College Station, TX (Ocean Drilling Program).

deMenocal, P., Bloemendal, J., and King, J., 1991. A rock-magnetic record of monsoonal dust deposition to the Arabian Sea: evidence for a shift in the mode of deposition at 2.4 Ma. *In* Prell, W.L., Niitsuma, N., et al., *Proc. ODP, Sci. Results*, 117: College Station, TX (Ocean Drilling Program), 389–407.

Emeis, K.-C., Robertson, A.H.F., Richter, C., et al., 1996. *Proc. ODP, Init. Repts.*, 160: College Station, TX (Ocean Drilling Program).

Farrell, J.W., and Janecek, T.R., 1991. Late Neogene paleoceanography and paleoclimatology of the northeast Indian Ocean (Site 758). *In* Weissel, J., Peirce, J., Taylor, E., Alt, J., et al., *Proc. ODP, Sci. Results*, 121: College Station, TX (Ocean Drilling Program), 297–355.

Hagelberg, T.K., Pisias, N.G., Shackleton, N.J., Mix, A.C., and Harris, S., 1995. Refinement of a high-resolution, continuous sedimentary section for studying equatorial Pacific Ocean paleoceanography, Leg 138. *In* Pisias, N.G., Mayer, L.A., Janecek, T.R., Palmer-Julson, A., and van Andel, T.H. (Eds.), *Proc. ODP, Sci Results*, 138: College Station, TX (Ocean Drilling Program), 31–46.

Murray, D.W., and Prell, W.L., 1991. Pliocene to Pleistocene variations in calcium carbonate, organic carbon, and opal on the Owen Ridge, northern Arabian Sea. *In* Prell, W.L., Niitsuma, N., et al., *Proc. ODP, Sci. Results*, 117: College Station, TX (Ocean Drilling Program), 343–363.

Paillard, D., 1996. Macintosh program performs time-series analysis. *Eos*, 77:379.

Raymo, M.E., Ruddiman, W.F., Backman, J., Clement, B.M., and Martinson, D.G., 1989. Late Pliocene variation in Northern Hemisphere ice sheets and North Atlantic deep water circulation. *Paleoceanography,* 4:413–446.

Rea, D.K., Basov, I.A., Janecek, T.R., Palmer-Julson, A., et al., 1993. *Proc. ODP, Init. Repts.*, 145: College Station, TX (Ocean Drilling Program).

Robinson, S.G., 1990. Applications for whole-core magnetic susceptibility measurements of deep-sea sediments: Leg 115 results. *In* Duncan, R.A., Backman, J., Peterson, L.C., et al., *Proc. ODP, Sci. Results*, 115: College Station, TX (Ocean Drilling Program), 737–771.

Ruddiman, W.F., Cameron, D., and Clement, B.M., 1987. Sediment disturbance and correlation of offset holes drilled with the hydraulic piston corer: Leg 94. *In* Ruddiman, W.F., Kidd, R.B., Thomas, E., et al., *Init. Repts. DSDP*, 94 (Pt. 2): Washington (U.S. Govt. Printing Office), 615–634.

Ruddiman, W.F., Raymo, M.E., Martinson, D.G., Clement, B.M., and Backman, J., 1989. Pleistocene evolution: Northern Hemisphere ice sheets and North Atlantic Ocean. *Paleoceanography,* 4:353–412.

Shackleton, N.J., Berger, A., and Peltier, W.A., 1990. An alternative astronomical calibration of the lower Pleistocene timescale based on ODP Site 677. *Trans. R. Soc. Edinburgh: Earth Sci.*, 81:251–261.

Shackleton, N.J., and Hall, M.A., 1983. Stable isotope record of Hole 504 sediments: high-resolution record of the Pleistocene. *In* Cann, J.R., Langseth, M.G., Honnorez, J., Von Herzen, R.P., White, S.M., et al. *Init. Repts. DSDP*, 69:431–441.

Date of initial receipt: 15 January 1997
Date of acceptance: 26 June 1997
Ms 160SR-053

Table 2. Coring gaps in Site 964.

Leg	Site	Hole	Core	Type	Top (mbsf)	Bottom (mbsf)	Top (rmcd)	Bottom (rmcd)	Length (mbsf)	Length (rmcd)	Distortion (%)	Coring gaps (mbsf)	Coring gaps (rmcd)
160	964	A	1	H	0.00	6.58	0.0000	6.5584	6.58	6.56	100%		
160	964	A	2	H	6.80	16.35	6.9484	16.4915	9.55	9.54	100%	0.22	0.39
160	964	A	3	H	16.30	25.88	17.0600	26.6200	9.58	9.56	100%	–0.05	0.57
160	964	A	4	H	25.80	35.46	27.5400	39.9000	9.66	12.36	128%	–0.08	0.92
160	964	A	5	H	35.30	45.02	40.6227	50.2400	9.72	9.62	99%	–0.16	0.72
160	964	A	6	H	44.80	54.48	51.0420	62.3182	9.68	11.28	116%	–0.22	0.80
160	964	A	7	H	54.30	63.97	63.4217	73.5283	9.67	10.11	105%	–0.18	1.10
160	964	A	8	H	63.80	73.50	74.6777	93.9882	9.70	19.31	199%	–0.17	1.15
160	964	A	9	H	73.30	82.46	94.9109	104.9349	9.16	10.02	109%	–0.2	0.92
160	964	A	10	H	82.80	92.48	105.7503	115.2753	9.68	9.53	98%	0.34	0.82
160	964	A	11	H	92.30	102.04	115.7794	126.3400	9.74	10.56	108%	–0.18	0.50
								Total:	102.72	118.44	115%	(0.68)	7.90
								Average:				(0.07)	0.79
								Percentage:				–1%	7%
160	964	B	1	H	0.00	7.85	0.0000	9.0658	7.85	9.07	115%		
160	964	B	2	H	8.10	17.69	9.0800	19.9210	9.59	10.84	113%	0.25	0.01
160	964	B	3	H	18.18	27.09	19.9200	29.1127	8.91	9.19	103%	0.49	0.00
160	964	B	4	H	27.10	36.65	30.1600	43.1267	9.55	12.97	136%	0.01	1.05
160	964	B	5	H	36.60	46.28	44.2000	53.7435	9.68	9.54	99%	–0.05	1.07
160	964	B	6	H	46.10	55.71	54.6384	64.1654	9.61	9.53	99%	–0.18	0.89
160	964	B	7	H	55.60	65.10	67.4257	77.0400	9.50	9.61	101%	–0.11	3.26
160	964	B	8	H	65.10	74.72	79.8374	89.6824	9.62	9.84	102%	0.00	2.80
160	964	B	9	H	74.60	84.17	90.6236	100.2886	9.57	9.67	101%	–0.12	0.94
160	964	B	10	H	84.10	93.67	105.0234	114.2030	9.57	9.18	96%	–0.07	4.73
160	964	B	11	H	93.60	102.01	114.8900	125.6971	8.41	10.81	129%	–0.07	0.69
								Total:	101.86	110.25	108%	0.15	15.45
								Average:				0.02	1.54
								Percentage:				0%	14%
160	964	C	6	H	43.10	52.80	55.2394	65.4022	9.70	10.16	105%		
160	964	C	7	H	52.60	62.14	66.0208	77.3229	9.54	11.30	118%	–0.20	0.62
160	964	C	8	H	62.10	71.10	78.5615	86.5146	9.00	7.95	88%	–0.04	1.24
160	964	C	9	H	71.60	81.29	87.8839	100.0160	9.69	12.13	125%	0.50	1.37
160	964	C	10	H	81.10	90.86	101.6207	114.7937	9.76	13.17	135%	–0.19	1.60
								Total:	47.69	54.72	115%	0.07	4.83
								Average:				0.02	1.21
								Percentage:				0%	9%
160	964	D	1	H	0.00	3.93	0.0000	5.3505	3.93	5.35	136%		
160	964	D	2	H	4.10	13.64	7.2757	16.3550	9.54	9.08	95%	0.17	1.93
160	964	D	3	H	13.60	23.21	17.1756	27.8957	9.61	10.72	112%	–0.04	0.82
160	964	D	4	H	23.10	32.73	28.4987	38.1067	9.63	9.61	100%	–0.11	0.60
160	964	D	5	H	32.60	41.96	38.8362	51.1000	9.36	12.26	131%	–0.13	0.73
160	964	D	6	H	42.10	51.71	52.2750	62.0250	9.61	9.75	101%	0.14	1.17
160	964	D	7	H	51.60	61.12	62.8110	75.4440	9.52	12.63	133%	–0.11	0.79
160	964	D	8	H	61.10	70.88	76.3771	86.4629	9.78	10.09	103%	–0.02	0.93
160	964	D	9	H	70.60	78.70	88.0500	96.4612	8.10	8.41	104%	–0.28	1.59
160	964	D	10	H	80.10	89.81	99.9773	108.3908	9.71	8.41	87%	1.40	3.52
160	964	D	11	H	89.60	99.40	114.8653	125.3525	9.80	10.49	107%	–0.21	6.47
160	964	D	12	H	99.10	108.84	125.5067	133.3150	9.74	7.81	80%	–0.30	0.15
								Total:	108.33	114.61	106%	0.51	18.70
								Average:				0.05	1.70
								Percentage:				0%	16%
160	964	E	1	H	0.00	5.30	0.0000	6.5750	5.30	6.58	124%		
160	964	E	2	H	5.50	15.14	11.0535	22.2660	9.64	11.21	116%	0.20	4.48
160	964	E	3	H	17.18	24.53	22.2800	29.9885	7.35	7.71	105%	2.04	0.01
160	964	E	4	H	57.00	66.73	69.9725	81.9520	9.73	11.98	123%	32.47	39.98
160	964	E	5	H	66.50	75.44	82.6550	94.6160	8.94	11.96	134%	–0.23	0.70
160	964	E	6	H	76.00	85.69	95.6400	106.6300	9.69	10.99	113%	0.56	1.02
								Total:	50.65	60.43	119%	35.04	6.22
								Average:				7.01	1.55
								Percentage:				69%	10%
160	964	F	1	H	0.00	9.00	0.9898	9.8320	9.00	8.84	98%		
								Total:	9.00	8.84	98%		
								Total:	420.25	467.29	111%	35.09	53.10
								Average:				0.00	1.31
								Percentage:				8%	11%

Table 3. Faulting and erosional gaps in Site 964.

Leg	Site	Hole	Core	Type	Section	Top (cm)	Bottom (cm)	Top (mbsf)	Bottom (mbsf)	Top (rmcd)	Bottom (rmcd)	Gaps (rmcd)
160	964	A	4	H	1	143	144	27.22	27.24	29.18	29.48	0.30
160	964	A	4	H	2	137	138	28.66	28.68	31.10	31.92	0.82
160	964	A	4	H	3	95	96	29.74	29.76	33.10	34.16	1.06
160	964	A	4	H	4	71	72	31.00	31.02	35.56	35.64	0.08
160	964	A	6	H	4	21	22	49.50	49.52	55.80	57.32	1.52
160	964	A	7	H	4	119	120	59.98	60.00	69.24	69.58	0.34
160	964	A	8	H	1	79	80	64.58	64.60	75.50	75.68	0.18
160	964	A	8	H	2	11	12	65.40	65.42	76.58	76.64	0.06
160	964	A	8	H	5	87	88	70.66	70.68	83.48	91.26	7.78
160	964	B	1	H	4	51	52	5.00	5.02	5.30	5.62	0.32
160	964	B	2	H	3	27	28	11.36	11.38	12.42	13.30	0.88
160	964	B	4	H	2	103	104	29.62	29.64	33.18	36.06	2.88
160	964	B	9	H	4	33	34	79.42	79.44	95.32	95.54	0.22
160	964	C	7	H	3	51	52	56.10	56.12	69.56	70.66	1.10
160	964	C	9	H	5	117	118	78.76	78.78	95.32	97.16	1.84
160	964	C	10	H	2	121	122	83.80	83.82	104.58	107.16	2.58
160	964	D	3	H	6	57	58	21.66	21.68	26.08	26.34	0.26
160	964	D	5	H	1	45	46	33.04	33.06	39.36	39.46	0.10
160	964	D	5	H	2	111	112	35.20	35.22	42.00	44.30	2.30
160	964	D	7	H	6	43	44	59.52	59.54	71.50	73.58	2.08*
160	964	D	9	H	1	75	76	71.34	71.36	88.86	89.70	0.84*
160	964	E	2	H	3	127	128	9.76	9.78	16.22	16.56	0.34
160	964	E	4	H	2	5	6	58.54	58.56	72.88	73.90	1.02*
160	964	E	5	H	5	37	38	72.86	72.88	89.62	91.26	1.64
160	964	E	6	H	1	83	84	76.82	76.84	96.48	97.14	0.66
											Total:	31.20
											Average:	1.25
											Maximum:	7.78
											Minimum:	0.06

Table 4. Revised composite depth section of Site 966.

Leg	Site	Hole	Core	Type	Section	Top	Bottom	mbsf	ties	leg	site	hole	core	type	section	top	bottom	mbsf	rmcd
160	966	B ↓	1	H	1	0.0	0.1	0.00											0.00
160	966	B	1	H	5	50.0	50.1	6.50	→	160	966	D ↓	2	H	3	28.0	28.1	6.78	6.50
160	966	B ↓	2	H	3	134.0	134.1	2.04	←	160	966	D	2	H	7	30.0	30.1	12.80	12.52
160	966	B	2	H	6	132.0	132.1	16.52	→	160	966	D ↓	3	H	2	76.0	76.1	15.26	17.00
160	966	B ↓	3	H	1	22.0	22.1	17.42	←	160	966	D	3	H	3	70.0	70.1	16.70	18.44
160	966	B	3	H	6	128.0	128.1	25.98	→	160	966	D ↓	4	H	1	120.0	120.1	23.70	27.00
160	966	B ↓	4	H	4	52.0	52.1	31.72	←	160	966	D	4	H	5	142.0	142.1	29.92	33.22
160	966	B	4	H	7	36.0	36.1	36.06	→	160	966	D ↓	5	H	2	10.0	10.1	33.60	37.56
160	966	B ↓	5	H	6	14.0	14.1	43.84	←	160	966	D	5	H	7	44.0	44.1	41.44	45.40
160	966	B	5	H	6	138.0	138.1	45.08	→	160	966	D ↓	6	H	1	62.0	62.1	42.12	46.64
160	966	B ↓	6	H	6	6.0	6.1	53.26	←	160	966	D	6	H	6	146.0	146.1	50.52	55.04
160	966	B	6	H	7	50.0	50.1	55.20	→	160	966	D ↓	7	H	1	90.0	90.1	51.90	56.98
160	966	B ↓	7	H	4	2.0	2.1	59.72	←	160	966	D	7	H	4	132.0	132.1	56.82	61.90
160	966	B	7	H	7	70.0	70.1	64.90											67.08

Table 5. Coring gaps in Site 966.

Leg	Site	Hole	Core	Type	Top (mbsf)	Bottom (mbsf)	Top (rmcd)	Bottom (rmcd)	Length (mbsf)	Length (rmcd)	Distortion (%)	Coring gaps (mbsf)	Coring gaps (rmcd)
160	966	A	1	H	0.00	5.48	0.00	5.80	5.48	5.80	106%		
160	966	A	2	H	5.80	14.00	7.66	17.08	8.20	9.42	115%	0.32	1.86
160	966	A	3	H	15.30	24.16	18.54	28.80	8.86	10.26	116%	1.30	1.46
160	966	A	4	H	24.80	34.23	29.82	40.25	9.43	10.43	111%	0.64	1.02
160	966	A	5	H	34.30	43.83	41.38	50.89	9.53	9.51	100%	0.07	1.13
160	966	A	6	H	43.80	53.45	52.60	64.09	9.65	11.49	119%	–0.03	1.71
160	966	A	7	H	53.30	62.86	65.50	67.08	9.56	1.58	17%	–0.15	1.41
								Total:	60.71	58.49	96%	2.15	8.59
								Average:			98%	0.36	1.43
								Percentage:				4%	15%
160	966	B	1	H	0.00	7.47	0.00	7.55	7.47	7.55	101%		
160	966	B	2	H	7.70	17.33	7.92	17.85	9.63	9.93	103%	0.23	0.37
160	966	B	3	H	17.20	26.90	18.22	27.78	9.70	9.56	99%	–0.13	0.37
160	966	B	4	H	26.70	36.33	28.56	37.85	9.63	9.29	96%	–0.20	0.78
160	966	B	5	H	36.20	45.85	38.44	47.31	9.65	8.87	92%	–0.13	0.59
160	966	B	6	H	45.70	55.26	47.80	57.06	9.56	9.26	97%	–0.15	0.49
160	966	B	7	H	55.20	64.93	57.72	67.11	9.73	9.39	97%	–0.06	0.66
								Total:	65.37	63.85	98%	(0.44)	3.26
								Average:			98%	–0.13	0.93
								Percentage:				–0.67%	5.11%
160	966	C	1	H	0.00	9.20	0.00	9.26	9.20	9.26	101%		
160	966	C	2	H	9.50	19.05	9.72	19.63	9.55	9.91	104%	0.30	0.46
160	966	C	3	H	19.00	28.67	20.08	30.09	9.67	10.01	104%	–0.05	0.45
160	966	C	4	H	28.50	38.04	30.26	39.94	9.54	9.68	101%	–0.17	0.17
160	966	C	5	H	38.00	47.61	40.38	49.59	9.61	9.21	96%	–0.04	0.44
160	966	C	6	H	47.50	57.15	50.12	58.69	9.65	8.57	89%	–0.11	0.53
160	966	C	7	H	57.00	66.65	59.74	67.11	9.65	7.37	76%	–0.15	1.05
								Total:	66.87	64.01	96%	(0.22)	3.10
								Average:			96%	–0.06	0.89
								Percentage:				–0.33%	4.84%
160	966	D	1	H	0.00	3.25	0.00	3.27	3.25	3.27	101%		
160	966	D	2	H	3.50	13.25	3.27	13.01	9.75	9.74	100%	0.25	0.00
160	966	D	3	H	13.00	22.71	14.54	24.61	9.71	10.07	104%	–0.25	1.53
160	966	D	4	H	22.50	32.06	25.68	35.54	9.56	9.86	103%	–0.21	1.07
160	966	D	5	H	32.00	41.65	35.66	45.59	9.65	9.93	103%	–0.06	0.12
160	966	D	6	H	41.50	51.03	45.96	55.65	9.53	9.69	102%	–0.15	0.37
160	966	D	7	H	51.00	60.67	56.06	65.97	9.67	9.91	102%	–0.03	0.41
160	966	D	8	H	60.50	63.50	66.00	67.09	3.00	1.09	36%	–0.17	0.03
								Total:	64.12	63.56	99%	(0.62)	3.53
								Average:			94%	–0.09	0.50
								Percentage:				–0.97%	5.56%
								Total:	257.07	249.91	97%	0.87	18.48
								Average:				0.02	0.94
								Percentage:				0.34%	7.40%

Table 6. Revised composite depth section of Site 967.

Leg	Site	Hole	Core	Type	Section	Top	Bottom	Depth (mbsf)	tie	Leg	Site	Hole	Core	Type	Section	Top	Bottom	Depth (mbsf)	Depth (rmcd)
160	967	D	1	H	1	2.0	2.1	0.02											0.02
		↓																	
160	967	D	1	H	5	24.0	24.1	6.24	→	160	967	C	1	H	4	98.0	98.1	5.48	6.16
160	967	B	2	H	3	56.0	56.1	8.86	←	160	967	C	1	H	7	30.0	30.1	9.30	9.98
		↓										↓							
160	967	B	2	H	4	118.0	118.1	10.98	→	160	967	C	2	H	1	110.0	110.1	10.60	12.10
												↓							
160	967	A	3	H	1	74.0	74.1	19.54	←	160	967	C	2	H	7	30.0	30.1	18.80	20.30
		↓																	
160	967	A	3	H	6	114.0	114.1	27.44	→	160	967	B	4	H	1	114.0	114.1	25.44	28.20
												↓							
160	967	A	4	H	2	90.0	90.1	30.70	←	160	967	B	4	H	4	58.0	58.1	29.38	32.14
		↓																	
160	967	A	4	H	7	18.0	18.1	37.48	→	160	967	B	5	H	2	38.0	38.1	35.68	38.92
												↓							
160	967	C	5	H	3	82.0	82.1	41.82	←	160	967	B	5	H	7	34.0	34.1	43.14	46.38
		↓																	
160	967	C	5	H	5	126.0	126.1	45.26	→	160	967	A	6	H	1	16.0	16.1	47.46	49.82
												↓							
160	967	C	6	H	1	38.0	38.1	47.88	←	160	967	A	6	H	3	42.0	42.1	50.72	53.08
		↓																	
160	967	C	6	H	4	6.0	6.1	52.06	→	160	967	B	7	H	1	64.0	64.1	53.44	57.26
												↓							
160	967	A	7	H	6	24.0	24.1	64.54	←	160	967	B	7	H	7	60.0	60.1	62.40	67.02
		↓																	
160	967	A	7	H	7	42.0	42.1	66.22	→	160	967	B	8	H	1	54.0	54.1	62.84	68.66
												↓							
160	967	A	8	H	3	68.0	68.1	69.98	←	160	967	B	8	H	4	48.0	48.1	67.28	73.10
		↓																	
160	967	A	8	H	6	102.0	102.1	74.82	→	160	967	C	7	H	5	142.0	142.1	64.42	77.94
												↓							
160	967	A	9	H	1	34.0	34.1	76.14	←	160	967	C	7	H	7	22.0	22.1	66.22	79.74
		↓																	
160	967	A	9	H	7	38.0	38.1	85.18	→	160	967	C	8	H	5	78.0	78.1	73.28	88.78
												↓							
160	967	A	10	H	2	14.0	14.1	86.94	←	160	967	C	8	H	6	128.0	128.1	75.28	90.78
		↓																	
160	967	A	10	H	7	60.0	60.1	94.90	→	160	967	C	9	H	4	120.0	120.1	81.70	98.74
												↓							
160	967	A	11	H	1	120.0	120.1	96.00	←	160	967	C	9	H	6	146.0	146.1	84.96	102.00
		↓																	
160	967	A	11	H	5	6.0	6.1	100.86	→	160	967	C	10	H	3	12.0	12.1	88.62	106.86
												↓							
160	967	A	12	H	2	42.0	42.1	106.22	←	160	967	C	10	H	6	106.0	106.1	94.06	112.30
		↓																	
160	967	A	12	H	6	68.0	68.1	112.48	→	160	967	C	11	H	5	2.0	2.1	101.02	118.54
												↓							
160	967	B	13	H	1	84.0	84.1	110.64	←	160	967	C	11	H	7	52.0	52.1	104.52	122.04
		↓																	
160	967	B	13	H	7	58.0	58.1	119.38											130.76

Table 7. Coring gaps in Site 967.

Leg	Site	Hole	Core	Type	Top (mbsf)	Bottom (mbsf)	Top (rmcd)	Bottom (rmcd)	Length (mbsf)	Length (rmcd)	Distortion (%)	Coring gaps (mbsf)	Coring gaps (rmcd)
160	967	A	1	H	0.00	9.05	0.00	9.27	9.05	9.27	102%		
160	967	A	2	H	9.30	18.85	10.14	18.95	9.55	8.81	92%	0.25	0.87
160	967	A	3	H	18.80	28.46	19.64	29.08	9.66	9.44	98%	–0.05	0.69
160	967	A	4	H	28.30	37.92	29.76	39.34	9.62	9.58	100%	–0.16	0.68
160	967	A	5	H	37.80	47.44	40.20	49.48	9.64	9.28	96%	–0.12	0.86
160	967	A	6	H	47.30	56.96	49.72	58.90	9.66	9.18	95%	–0.14	0.24
160	967	A	7	H	56.80	66.24	58.92	68.74	9.44	9.82	104%	–0.16	0.02
160	967	A	8	H	66.30	76.00	69.66	79.02	9.70	9.36	96%	0.06	0.92
160	967	A	9	H	75.80	85.42	79.48	89.00	9.62	9.52	99%	–0.20	0.46
160	967	A	10	H	85.30	95.00	89.54	98.88	9.70	9.34	96%	–0.12	0.54
160	967	A	11	H	94.80	104.56	100.44	110.42	9.76	9.98	102%	–0.20	1.56
160	967	A	12	H	104.30	112.95	110.70	118.93	8.65	8.23	95%	–0.26	0.28
160	967	A	13	H	113.80	120.12	122.80	127.94	6.32	5.14	81%	0.85	3.87
								Total:	120.37	116.96	97%	–0.25	10.98
								Average:			97%	–0.02	0.92
								Percentage:				–0.2%	9.4%
160	967	B	1	H	0.00	5.08	0.00	5.14	5.08	5.14	101%		
160	967	B	2	H	5.30	14.98	5.98	15.92	9.68	9.94	103%	0.22	0.84
160	967	B	3	H	14.80	24.44	16.52	26.14	9.64	9.62	100%	–0.18	0.60
160	967	B	4	H	24.30	34.00	27.12	36.82	9.70	9.70	100%	–0.14	0.98
160	967	B	5	H	33.80	43.47	37.08	46.67	9.67	9.59	99%	–0.20	0.26
160	967	B	6	H	43.30	53.00	47.92	56.06	9.70	8.14	84%	–0.17	1.25
160	967	B	7	H	52.80	62.43	56.64	67.05	9.63	10.41	108%	–0.20	0.58
160	967	B	8	H	62.30	71.99	68.36	78.11	9.69	9.75	101%	–0.13	1.31
160	967	B	9	H	71.80	81.47	79.04	89.65	9.67	10.61	110%	–0.19	0.93
160	967	B	10	H	81.30	91.02	91.14	101.70	9.72	10.56	109%	–0.17	1.49
160	967	B	11	H	90.80	100.45	102.80	112.47	9.65	9.67	100%	–0.22	1.10
160	967	B	12	H	100.30	108.92	112.60	121.08	8.62	8.48	98%	–0.15	0.13
160	967	B	13	H	109.80	116.12	121.22	127.50	6.32	6.28	99%	0.88	0.14
								Total:	116.77	117.89	101%	–0.65	9.61
								Average:			101%	–0.05	0.80
								Percentage:				–0.6%	8.2%
160	967	C	1	H	0.00	9.63	0.00	10.23	9.63	10.23	106%		
160	967	C	2	H	9.50	19.12	11.24	20.64	9.62	9.40	98%	–0.13	1.01
160	967	C	3	H	19.00	28.79	21.26	31.38	9.79	10.12	103%	–0.12	0.62
160	967	C	4	H	28.50	38.23	31.39	41.21	9.73	9.82	101%	–0.29	0.01
160	967	C	5	H	38.00	47.75	42.12	52.43	9.75	10.31	106%	–0.23	0.91
160	967	C	6	H	47.50	57.20	52.76	68.34	9.70	15.58	161%	–0.25	0.33
160	967	C	7	H	57.00	66.72	69.50	80.34	9.72	10.84	112%	–0.20	1.16
160	967	C	8	H	66.50	76.22	81.02	91.80	9.72	10.78	111%	–0.22	0.68
160	967	C	9	H	76.00	85.62	93.04	102.80	9.62	9.76	101%	–0.22	1.24
160	967	C	10	H	85.50	95.31	103.80	113.55	9.81	9.75	99%	–0.12	1.00
160	967	C	11	H	95.00	104.73	113.62	122.39	9.73	8.77	90%	–0.31	0.07
160	967	C	12	H	104.50	109.00	122.90	127.22	4.50	4.32	96%	–0.23	0.51
								Total	111.32	119.68	108%	–2.32	7.54
								Average			107%	–0.21	0.69
								Percentage:				–2.1%	6.3%
160	967	D	1	H	0.00	9.63	0.00	9.61	9.63	9.61	100%		
								Total:	9.63	9.61	100%		
								Average:			100%		
								Percentage:					
								Total:	358.09	364.13	102%	–3.22	28.14
								Average:				–0.10	0.80
								Percentage:				–1%	8%

Table 8. Revised composite depth section of Site 969.

Leg	Site	Hole	Core	Type	Section	Top	Bottom	Depth (mbsf)	ties	Leg	Site	Hole	Core	Type	Section	Top	Bottom	Depth (mbsf)	Depth (rmcd)
160	969	D	1	H	1	0.0	0.1	0.00											0.00
		↓																	
160	969	D	1	H	6	20.0	20.1	7.70	→	160	969	A	2	H	1	84.0	84.1	8.54	7.70
												↓							
160	969	D	2	H	1	50.0	50.1	9.40	←	160	969	A	2	H	2	76.0	76.1	9.96	9.12
		↓																	
160	969	D	2	H	7	50.0	50.1	18.40	→	160	969	B	3	H	3	16.0	16.1	15.56	18.12
												↓							
160	969	D	3	H	1	84.0	84.1	19.24	←	160	969	B	3	H	4	2.0	2.1	16.92	19.48
		↓																	
160	969	D	3	H	7	42.0	42.1	27.82	→	160	969	B	4	H	1	58.0	58.1	22.48	28.06
												↓							
160	969	D	4	H	1	84.0	84.1	28.74	←	160	969	B	4	H	2	56.0	56.1	23.96	29.54
		↓																	
160	969	D	4	H	7	26.0	26.1	37.16	→	160	969	B	4	H	6	66.0	66.1	30.06	37.96
												↓							
160	969	D	5	H	1	28.0	28.1	37.68	←	160	969	B	4	H	6	106.0	106.1	30.46	38.36
		↓																	
160	969	D	5	H	7	20.0	20.1	46.60	→	160	969	B	5	H	2	124.0	124.1	34.14	46.74
												↓							
160	969	D	6	H	1	138.0	138.1	48.28	←	160	969	B	5	H	3	72.0	72.1	35.12	47.72
		↓																	
160	969	D	6	H	6	102.0	102.1	55.42	→	160	969	A	5	H	3	114.0	114.1	40.34	54.58
												↓							
160	969	D	7	H	1	82.0	82.1	57.22	←	160	969	A	5	H	4	60.0	60.1	41.30	55.54
		↓																	
160	969	D	7	H	6	144.0	144.1	65.34	→	160	969	B	6	H	3	60.0	60.1	44.50	63.25
												↓							
160	969	D	8	H	1	14.0	14.1	66.04	←	160	969	B	6	H	3	118.0	118.1	45.08	63.85
		↓																	
160	969	D	8	H	6	136.0	136.1	74.76	→	160	969	E	6	H	5	64.0	64.1	49.54	72.05
												↓							
160	969	D	9	H	1	6.0	6.1	75.46	←	160	969	E	6	H	6	96.0	96.1	51.36	73.87
		↓																	
160	969	D	9	H	7	2.0	2.1	84.42	→	160	969	E	7	H	2	148.0	148.1	55.38	81.35
												↓							
160	969	A	8	H	1	38.0	38.1	65.08	←	160	969	E	7	H	6	142.0	142.1	61.32	87.31
		↓																	
160	969	A	8	H	5	138.0	138.1	72.08	→	160	969	E	8	H	4	124.0	124.1	67.64	94.31
												↓							
160	969	B	9	H	1	146.0	146.1	70.86	←	160	969	E	8	H	7	30.0	30.1	71.20	97.87
		↓																	
160	969	B	9	H	4	30.0	30.1	74.20	→	160	969	E	9	H	1	36.0	36.1	71.76	101.21
												↓							
160	969	B	10	H	1	32.0	32.1	79.22	←	160	969	E	9	H	5	14.0	14.1	77.54	106.99
		↓																	
160	969	B	10	H	3	128.0	128.1	83.18	→	160	969	E	10	H	1	118.0	118.1	82.08	110.95
												↓							
160	969	A	10	H	1	56.0	56.1	84.26	←	160	969	E	10	H	2	24.0	24.1	82.64	111.51
		↓																	
160	969	A	10	H	2	146.0	146.1	86.66	→	160	969	D	13	H	1	124.0	124.1	113.24	113.91
												↓							
160	969	A	10	H	3	122.0	122.1	87.92	←	160	969	D	13	H	3	46.0	46.1	115.46	115.89
		↓																	
160	969	A	10	H	7	60.0	60.1	93.30											121.27
		↓																	
160	969	A	11	H	1	4.0	4.1	93.24											121.43
		↓																	
160	969	A	11	H	5	120.0	120.1	100.40	→	160	969	B	11	H	5	104.0	104.1	95.44	128.59
												↓							
										160	969	B	11	H	7	60.0	60.1	98.00	131.15

Table 9. Coring gaps in Site 969.

Leg	Site	Hole	Core	Type	Top (mbsf)	Bottom (mbsf)	Top (rmcd)	Bottom (rmcd)	Length (mbsf)	Length (rmcd)	Distortion (%)	Coring gaps (mbsf)	Coring gaps (rmcd)
160	969	A	1	H	0.00	7.40	0.0000	6.7764	7.40	6.78	92%		
160	969	A	2	H	7.70	17.30	7.0238	18.2211	9.60	11.20	117%	0.30	0.25
160	969	A	3	H	17.20	26.79	18.8445	32.3525	9.59	13.51	141%	–0.10	0.62
160	969	A	4	H	26.70	36.24	33.6956	47.8112	9.54	14.12	148%	–0.09	1.34
160	969	A	5	H	36.20	45.75	48.1292	61.3912	9.55	13.26	139%	–0.04	0.32
160	969	A	6	H	45.70	55.27	62.5098	74.0532	9.57	11.54	121%	–0.05	1.12
160	969	A	7	H	55.20	64.09	75.2177	85.7021	8.89	10.48	118%	–0.07	1.16
160	969	A	8	H	64.70	74.37	86.9105	97.0418	9.67	10.13	105%	0.61	1.21
160	969	A	9	H	74.20	83.89	98.9158	109.2624	9.69	10.35	107%	–0.17	1.87
160	969	A	10	H	83.70	93.31	110.8062	121.2420	9.61	10.44	109%	–0.19	1.54
160	969	A	11	H	93.20	100.70	121.4502	128.8727	7.50	7.42	99%	–0.11	0.21
								Total:	100.61	119.22	119%	0.09	9.65
								Average:				0.01	0.96
								Percentage:				0%	8%
160	969	B	1	H	0.00	2.72	0.0000	2.4743	2.72	2.47	91%		
160	969	B	2	H	2.90	12.48	3.0130	11.3854	9.58	8.37	87%	0.18	0.54
160	969	B	3	H	12.40	21.91	15.0926	27.2305	9.51	12.14	128%	–0.08	3.71
160	969	B	4	H	21.90	31.48	27.6457	39.6720	9.58	12.03	126%	–0.01	0.42
160	969	B	5	H	31.40	40.98	40.8943	56.0878	9.58	15.19	159%	–0.08	1.22
160	969	B	6	H	40.90	50.55	58.1636	71.2727	9.65	13.11	136%	–0.08	2.08
160	969	B	7	H	50.40	59.35	73.0064	84.5005	8.95	11.49	128%	–0.15	1.73
160	969	B	8	H	59.90	68.62	85.6316	94.3463	8.72	8.71	100%	0.55	1.13
160	969	B	9	H	69.40	78.40	96.1666	105.3624	9.00	9.20	102%	0.78	1.82
160	969	B	10	H	78.90	83.40	106.5423	111.1276	4.50	4.59	102%	0.50	1.18
160	969	B	11	H	94.40	98.01	127.9619	131.1640	3.61	3.20	89%		
								Total:	85.40	100.51	118%	1.61	13.82
								Average:				0.18	1.54
								Percentage:				2%	14%
160	969	C	1	H	0.02	9.60	3.3077	12.6818	9.58	9.37	98%		
								Total:	9.58	9.37	98%		
160	969	D	1	H	0.00	8.69	0.0000	8.5043	8.69	8.50	98%		
160	969	D	2	H	8.90	18.53	8.5992	18.2240	9.63	9.62	100%	0.21	0.09
160	969	D	3	H	18.40	28.02	18.6991	28.1744	9.62	9.48	98%	–0.13	0.48
160	969	D	4	H	27.90	37.46	28.9254	38.1200	9.56	9.19	96%	–0.12	0.75
160	969	D	5	H	37.40	46.94	38.2308	46.9848	9.54	8.75	92%	–0.06	0.11
160	969	D	6	H	46.90	56.64	47.0551	54.9667	9.74	7.91	81%	–0.04	0.07
160	969	D	7	H	56.40	65.40	55.0467	63.2925	9.00	8.25	92%	–0.24	0.08
160	969	D	8	H	65.90	75.65	63.6899	72.5674	9.75	8.88	91%	0.50	0.40
160	969	D	9	H	75.40	84.78	73.7800	81.7327	9.38	7.95	85%	–0.25	1.21
160	969	D	10	H	84.90	94.66	82.5616	90.1664	9.76	7.60	78%	0.12	0.83
160	969	D	11	H	94.40	103.97	90.3586	97.7846	9.57	7.43	78%	–0.26	0.19
160	969	D	12	H	103.90	111.64	99.5266	110.2654	7.74	10.74	139%	–0.07	1.74
160	969	D	13	H	112.00	115.84	113.1401	116.3140	3.84	3.17	83%	0.36	2.87
								Total:	115.82	107.48	93%	0.02	8.83
								Average:				0.00	0.74
								Percentage:				0%	8%
160	969	E	1	H	0.00	4.50	0.0000	3.9600	4.50	3.96	88%		
160	969	E	2	H	4.90	14.49	4.4426	15.3755	9.59	10.93	114%	0.40	0.48
160	969	E	3	H	14.40	23.96	18.8051	30.0815	9.56	11.28	118%	–0.09	3.43
160	969	E	4	H	23.90	33.54	31.0250	45.4100	9.64	14.39	149%	–0.06	0.94
160	969	E	5	H	33.40	42.93	46.7557	61.0801	9.53	14.32	150%	–0.14	1.35
160	969	E	6	H	42.90	52.61	63.1777	75.7355	9.71	12.56	129%	–0.03	2.10
160	969	E	7	H	52.40	61.81	77.4271	87.6538	9.41	10.23	109%	–0.21	1.69
160	969	E	8	H	61.90	71.24	88.8316	97.9116	9.34	9.08	97%	0.09	1.18
160	969	E	9	H	71.40	80.10	100.7880	108.3276	8.70	7.54	87%	0.16	2.88
160	969	E	10	H	80.90	88.10	109.9343	117.2328	7.20	7.30	101%	0.80	1.61
160	969	E	11	H	88.40	96.40	117.3552	131.1540	8.00	13.80	172%	0.30	0.12
								Total:	95.18	115.38	121%	1.22	15.77
								Average:				0.12	1.58
								Percentage:				1%	14%
160	969	F	1	H	0.00	9.36	0.0000	11.7688	9.36	11.77	126%		
								Total:	9.36	11.77	126%		
								Total:	415.95	463.74	111%	2.94	48.08
								Average:				0.08	1.20
								Percentage:				1%	10%

Table 10. Faulting and erosional gaps in Site 969.

Leg	Site	Hole	Core	Type	Section	Top (cm)	Bottom (cm)	Depth Top (mbsf)	Depth Bottom (mbsf)	Depth Top (rmcd)	Depth Bottom (rmcd)	Gaps (rmcd)
160	969	A	2	H	6	51	52	15.70	15.72	14.73	16.74	2.01
160	969	A	3	H	3	21	22	20.40	20.42	21.94	24.82	2.88
160	969	A	3	H	4	57	58	22.26	22.28	26.79	27.48	0.69
160	969	A	3	H	6	49	50	25.18	25.20	30.02	30.44	0.42
160	969	A	8	H	6	41	42	72.60	72.62	94.83	95.33	0.50
160	969	A	9	H	2	129	130	76.98	77.00	100.83	101.91	1.08
160	969	A	9	H	7	17	18	83.36	83.38	107.87	108.71	0.84
160	969	A	10	H	3	47	48	87.16	87.18	114.73	115.03	0.30
160	969	B	3	H	5	31	32	18.70	18.72	21.12	24.04	2.92
160	969	B	5	H	5	137	138	38.76	38.78	53.45	54.08	0.63
160	969	D	12	H	1	55	56	104.44	104.46	100.17	103.83	3.66
160	969	D	12	H	3	43	44	107.32	107.34	106.47	107.31	0.84
160	969	E	2	H	5	115	116	12.04	12.06	10.66	12.86	2.20
160	969	E	3	H	3	7	8	17.46	17.48	21.62	24.56	2.94
160	969	E	6	H	2	91	92	45.30	45.32	65.19	65.77	0.58
160	969	E	11	H	3	85	86	92.24	92.26	120.75	126.07	5.32
160	969	E	11	H	6	23	24	96.12	96.14	128.93	130.65	1.72
160	969	F	1	H	5	7	8	6.06	6.08	5.97	6.82	0.85
											Total:	30.39
											Average:	1.69
											Maximum:	5.32
											Minimum:	0.30

Table 11. Dips of inclination of Hole 969D.

Core	Inclination (°)
160-969D-	
5H	19.7
6H	16.3
7H	18.0
8H	19.7
9H	33.2
10H	34.9
11H	36.6
12H	32.1
13H	27.6
Average	25.6